Chemical Science

ROYAL SOCIETY OF CHEMISTRY

EDGE ARTICLE

View Article Online
View Journal | View Issue

Cite this: *Chem. Sci.*, 2023, **14**, 4845

All publication charges for this article have been paid for by the Royal Society of Chemistry

Isoamphipathic antibacterial molecules regulating activity and toxicity through positional isomerism†

Swagatam Barman,[a] Sudip Mukherjee,[a] Logia Jolly,[a] Cassandra Troiano,[b] Alessandro Grottesi,[c] Debajyoti Basak,[a] Paolo Calligari,[b] Brinta Bhattacharjee,[a] Gianfranco Bocchinfuso,[b] Lorenzo Stella[b] and Jayanta Haldar[*ad]

Peptidomimetic antimicrobials exhibit a selective interaction with bacterial cells over mammalian cells once they have achieved an optimum amphiphilic balance (hydrophobicity/hydrophilicity) in the molecular architecture. To date, hydrophobicity and cationic charge have been considered the crucial parameters to attain such amphiphilic balance. However, optimization of these properties is not enough to circumvent unwanted toxicity towards mammalian cells. Hence, herein, we report new isoamphipathic antibacterial molecules (IAMs: **1–3**) where positional isomerism was introduced as one of the guiding factors for molecular design. This class of molecules displayed good (MIC = 1–8 μg mL^{-1} or μM) to moderate [MIC = 32–64 μg mL^{-1} (32.2–64.4 μM)] antibacterial activity against multiple Gram-positive and Gram-negative bacteria. Positional isomerism showed a strong influence on regulating antibacterial activity and toxicity for *ortho* [IAM-**1**: MIC = 1–32 μg mL^{-1} (1–32.2 μM), HC_{50} = 650 μg mL^{-1} (654.6 μM)], *meta* [IAM-**2**: MIC = 1–16 μg mL^{-1} (1–16.1 μM), HC_{50} = 98 μg mL^{-1} (98.7 μM)] and *para* [IAM-**3**: MIC = 1–16 μg mL^{-1} (1–16.1 μM), HC_{50} = 160 μg mL^{-1} (161.1 μM)] isomers. Co-culture studies and investigation of membrane dynamics indicated that *ortho* isomer, IAM-**1** exerted more selective activity towards bacterial over mammalian membranes, compared to *meta* and *para* isomers. Furthermore, the mechanism of action of the lead molecule (IAM-**1**) has been characterized through detailed molecular dynamics simulations. In addition, the lead molecule displayed substantial efficacy against dormant bacteria and mature biofilms, unlike conventional antibiotics. Importantly, IAM-**1** exhibited moderate *in vivo* activity against MRSA wound infection in a murine model with no detectable dermal toxicity. Altogether, the report explored the design and development of isoamphipathic antibacterial molecules to establish the role of positional isomerism in achieving selective and potential antibacterial agents.

Received 3rd November 2022
Accepted 5th April 2023

DOI: 10.1039/d2sc06065e

rsc.li/chemical-science

Introduction

The rapid emergence of antimicrobial resistance (AMR) and chronic and recurrent infections owing to bacterial biofilm formation and predominance of dormant bacterial subpopulation are accountable for huge global mortality.[1–9] Another concern is a declining arsenal in antibiotic pipelines.[10,11] Hence, various organizations, including the World Health Organization, raised the alarm for the urgent development of a new class of antimicrobial agents.[12] Towards this aim, bacterial membrane targeting peptidomimetic antimicrobials have received significant attention, particularly because of the slower development of bacterial resistance against them.[13–26] Nevertheless, these peptidomimetic molecules often suffer from unwanted toxicity toward mammalian cells. Various research groups, including ours, observed that in general, an increment in hydrophobicity in any peptidomimetic molecular design is associated with toxic effects.[13–16,18–27,40] On the other side, the reduction in overall hydrophobicity produces less toxic molecules with compromised antibacterial efficacy. Thus, studying a new parameter for the fine structural tuning of peptidomimetic antibacterial molecules has significant relevance.

Towards this goal, herein, we report new isoamphipathic antibacterial molecules (IAMs: **1–3**), based on our previous design.[26] This class of molecules (IAMs) consists of phenylalanine residues, two cationic charges, confined alkyl spacers (in between two positively charged centres), non-peptide amide

[a]*Antibacterial Research Laboratory, New Chemistry Unit, Jawaharlal Nehru Centre for Advanced Scientific Research (JNCASR), Jakkur, Bangalore, 560064, India. E-mail: jayanta@jncasr.ac.in*

[b]*Department of Chemical Science and Technologies, University of Rome Tor Vergata, via della Ricerca Scientifica, 1, 00133, Rome, Italy*

[c]*Cineca, Via dei Tizii, 6, 00185, Rome, Italy*

[d]*School of Advanced Materials, Jawaharlal Nehru Centre for Advanced Scientific Research (JNCASR), Jakkur, Bangalore, 560064, India*

† Electronic supplementary information (ESI) available: The detailed synthetic protocol, molecular characterization, protocols for biological assays and theoretical studies, and supporting figures. See DOI: https://doi.org/10.1039/d2sc06065e

linkages, and pendant ester functionalities (Fig. 1A). An additional aromatic diol (*ortho*: catechol, *meta*: resorcinol, and *para*: hydroquinone) was incorporated in the confined alkyl spacer region to introduce positional isomerism in the molecular architecture. This resulted in three positional isomers IAM-**1** (*ortho*), IAM-**2** (*meta*), and IAM-**3** (*para*). Herein, pendant ester functionalities were fixed to an ethyl moiety, since they did not exhibit much detrimental effect on mammalian cells, in our previous design of the ASAM series.[26] In this article, first, molecular dynamics simulations with IAMs: **1–3** were performed to understand the conformation of the isomers in aqueous solution. The antibacterial and hemolytic activities of IAMs **1–3** were evaluated against various bacterial strains and human erythrocytes (hRBCs) showing the importance of positional isomerism in controlling selective interactions with the bacterial envelope over the mammalian membrane. To strengthen the influence of positional isomerism on IAM activity/selectivity, co-culture studies where bacteria and mammalian cells (hRBC RAW cells) were simultaneously present, were conducted. Furthermore, biophysical studies were

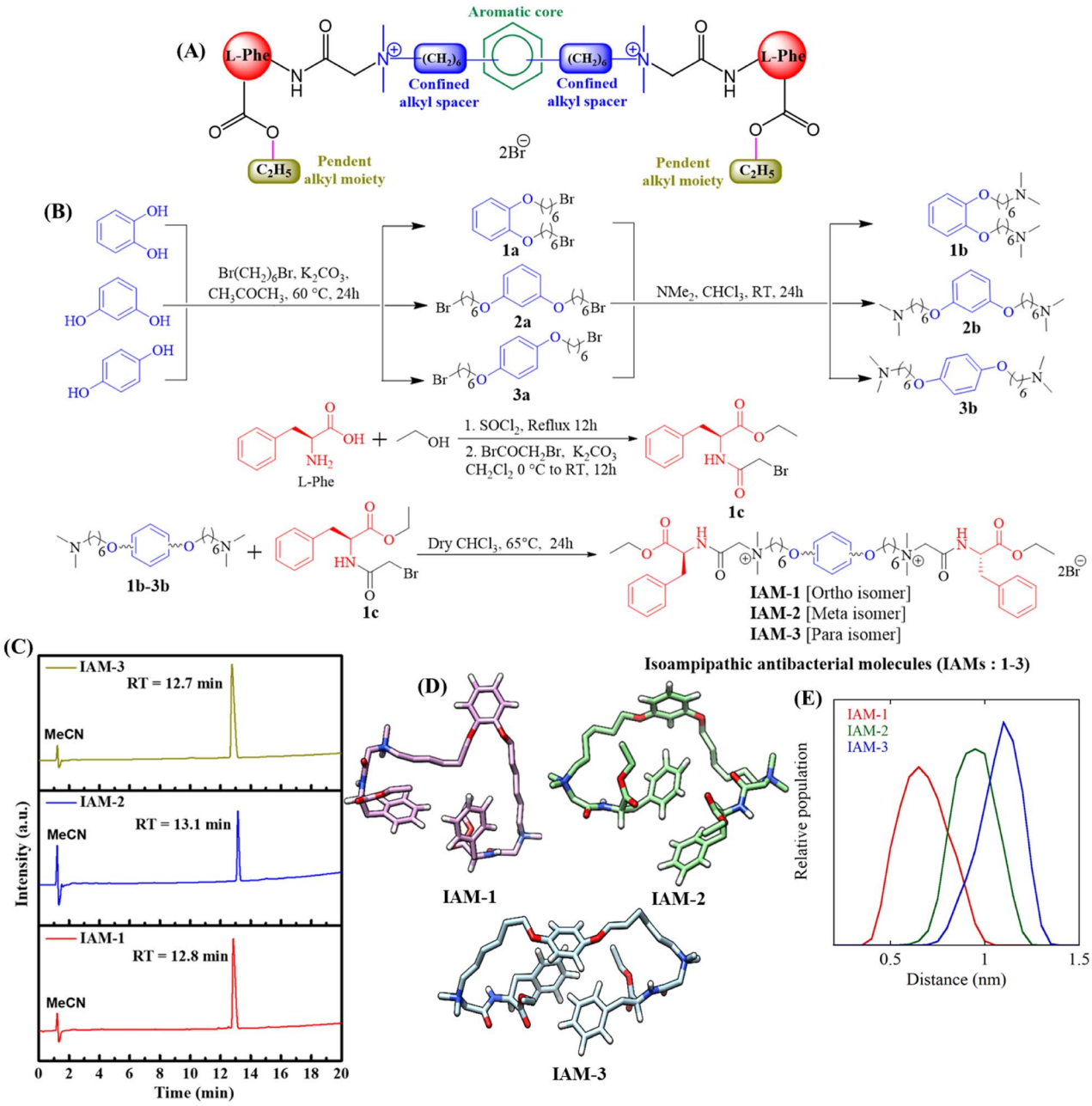

Fig. 1 (A) Schematic of molecular design of IAMs; (B) synthesis of isoamphipathic antibacterial molecules (IAMs: **1–3**); (C) amphiphilicity of IAMs: **1–3** through HPLC retention time measurement; (D) representative structures obtained from the simulations of the three compounds in aqueous solution (pink, IAM-**1**, green, IAM-**2**, and light blue, IAM-**3**) and (E) distance between the centres of mass of the two C6 alkyl chains, obtained from the simulation.

performed with IAMs **1–3** in model bacterial and mammalian membranes to monitor the change in membrane dynamics/fluidity and the extent of membrane leakage with respect to positional isomerism. Based on the overall biological and biophysical studies, *ortho*-isomer IAM-**1** was selected as the lead molecule. Furthermore, bactericidal kinetics, anti-stationary and anti-persister activity, as well as anti-biofilm efficacy of IAM-**1**, were investigated in detail. In addition, the membrane-active mechanism of bacterial killing was studied with IAM-**1**, through fluorescence spectroscopy and microscopy studies. Furthermore, the interaction of IAM-**1** with model bacterial membranes was studied through molecular dynamics simulations using the minimum bias approach.

Results and discussion

Design and synthesis

Our designed molecules are small molecular mimetics of antimicrobial peptides (AMPs), a part of the human innate immune system.[28,29] In the molecular structure, the central aromatic core, confined alkyl spacers, pendent ester chains, and amino acid side chains contribute as hydrophobic domains. The quaternary amine charges and ether, ester, and non-peptidic amide linkages contribute as hydrophilic counterparts. The core aromatic moiety introduced positional isomerism in the molecular design (Fig. 1A). Herein, isoamphipathic antibacterial molecules (IAMs **1–3**) were synthesized by following four simple synthetic steps, as outlined in Fig. 1B. First, aromatic diols (catechol, resorcinol, and hydroquinone) were individually reacted with dibromohexane under mild basic conditions to obtain dibromohexyloxy benzenes (**1a**, **2a**, and **3a**). Furthermore, dimethyl amine was reacted with dibromohexyloxy benzene intermediates at room temperature, to produce *N*,*N*,*N*′,*N*′-tetramethyl diaminohexyloxy benzenes (**1b**, **2b**, and **3b**). On the other side, the free acid group of L-phenylalanine was esterified under refluxing conditions using ethanol. The crude products originating from the esterification reaction were further reacted with bromoacetyl bromide under basic conditions to obtain the activated ethyl ester bromide derivatives of phenylalanine (**1c**). To this end, different *N*,*N*,*N*′,*N*′-tetramethyl diaminohexyloxy benzenes (**1b**, **2b**, and **3b**) were quaternized with the activated ethyl ester bromide derivatives of phenylalanine (**1c**) to synthesize all the final molecules (IAMs **1–3**) with quantitative yield. All the intermediates and IAMs were characterized thoroughly through ^{1}H-NMR, ^{13}C-NMR, and HRMS (ESI, Fig. S1–S9†). Importantly, all these isomers (IAMs: **1–3**) showed similar retention times (12.7–13.1 min) in HPLC indicating their isoamphipathic nature (Fig. 1C).

Furthermore, to analyse the conformations of the three IAMs in solution, we performed three independent simulations for each compound in water (four in the case of IAM-**1**), in the presence of a physiological salt concentration, for a total of almost 12 microseconds. Overall, the simulations revealed that all the isomers were extremely flexible and dynamic. Fig. 1D reports the most representative conformation for each of the three compounds. Herein, the different attachment of the two "arms" to the central aromatic moiety determined a different relative arrangement of the confined hexyl chains. In particular, for the *ortho* analogue (IAM-**1**) the two hexyl groups were on average closer to each other compared to the other two isomers (Fig. 1E).

Antibacterial and hemolytic activity

The antibacterial activity and hemolytic activity of all the IAMs **1–3** were evaluated against various Gram-positive and Gram-negative bacteria including multi-drug resistant clinical isolates and human red blood cells (hRBCs) respectively through the broth dilution method (Fig. 2A and ESI Table 1†). The antibacterial activity was expressed in terms of minimum inhibitory concentration (MIC) (concentration of the test compound required for complete inhibition of bacterial growth). Hemolytic activity was presented as HC_{50} (concentration of the test compound accountable for 50% lysis of hRBCs). The isomers displayed moderate to good antibacterial activity [*ortho* isomer: IAM-**1**; MIC = 1–64 μg mL^{-1} (1–64.4 μM), *meta* isomer: IAM-**2**; MIC = 1–16 μg mL^{-1} (1–16.1 μM) and *para* isomer: IAM-**3**; MIC = 1–16 μg mL^{-1} (1–16.1 μM)]. Upon testing against Gram-positive bacteria (*S. epidermidis*, *S. aureus*, MRSA, VRSA, and *E. faecium*), all three positional isomers, IAMs **1–3** completely inhibited bacterial growth at almost similar concentrations with the MIC ranging from 1–8 μg mL^{-1} or μM. Importantly, all these isomers were active against Gram-negative bacterial species. In the case of *E. coli*, the compounds exhibited MIC values in the range of 4–16 μg mL^{-1} (4–16.1 μM). Although these isomeric molecules (IAMs **1–3**) did not display a drastic difference in antibacterial activity, they showed a remarkable differentiation with respect to the hemolytic activity. The *ortho* isomer, IAM-**1** exhibited a much higher HC_{50} value of 650 μg mL^{-1} (654.6 μM) compared to *meta*-isomer, IAM-**2** [HC_{50} = 98 μg mL^{-1} (98.7 μM)], and *para*-isomer, IAM-**3** [HC_{50} = 160 μg mL^{-1} (161.1 μM)] (Fig. 2A and ESI Table 1†). At a concentration of 256 μg mL^{-1} (257.8 μM) (*i.e.* much higher than the MIC values), the extent of hRBC lysis for IAM-**1** was only 13% whereas for IAM-**2** and IAM-**3** it was >80% (Fig. 2B). This suggested that the toxicity profile rather than the antibacterial activity of phenylalanine and hexyl bearing compounds, IAMs **1–3** was strongly influenced by positional isomerism. Furthermore, to understand the impact of positional isomerism, the selectivity index (HC_{50}/MIC) was calculated for IAMs **1–3** against all the tested Gram-positive and Gram-negative bacteria. Fig. 2C reveals that IAM-**1** showed 650 fold, 162 fold, and 81 fold selectivity against *S. epidermidis*, MRSA and *E. faecium* respectively over human erythrocytes. In contrast, 98–160 fold, 40–49 fold, and 41–49 fold selectivity against *S. epidermidis*, MRSA, and *E. faecium* respectively were displayed by the other two isomers, IAM-**2** and IAM-**3** over human erythrocytes. In the cases of *S. aureus*, VRSA, *E. coli,* and *A. baumannii*, the *ortho* (IAM-**1**) and *para* (IAM-**2**) isomers showed similar selectivity while *meta*- (IAM-**3**) isomer's selectivity was quite low. Altogether, all three isomers showed a good selectivity index. More interestingly, the *ortho* isomer, IAM-**1** showed superior selectivity towards bacteria over mammalian cells in comparison to the *meta* and *para* isomers. Based on the

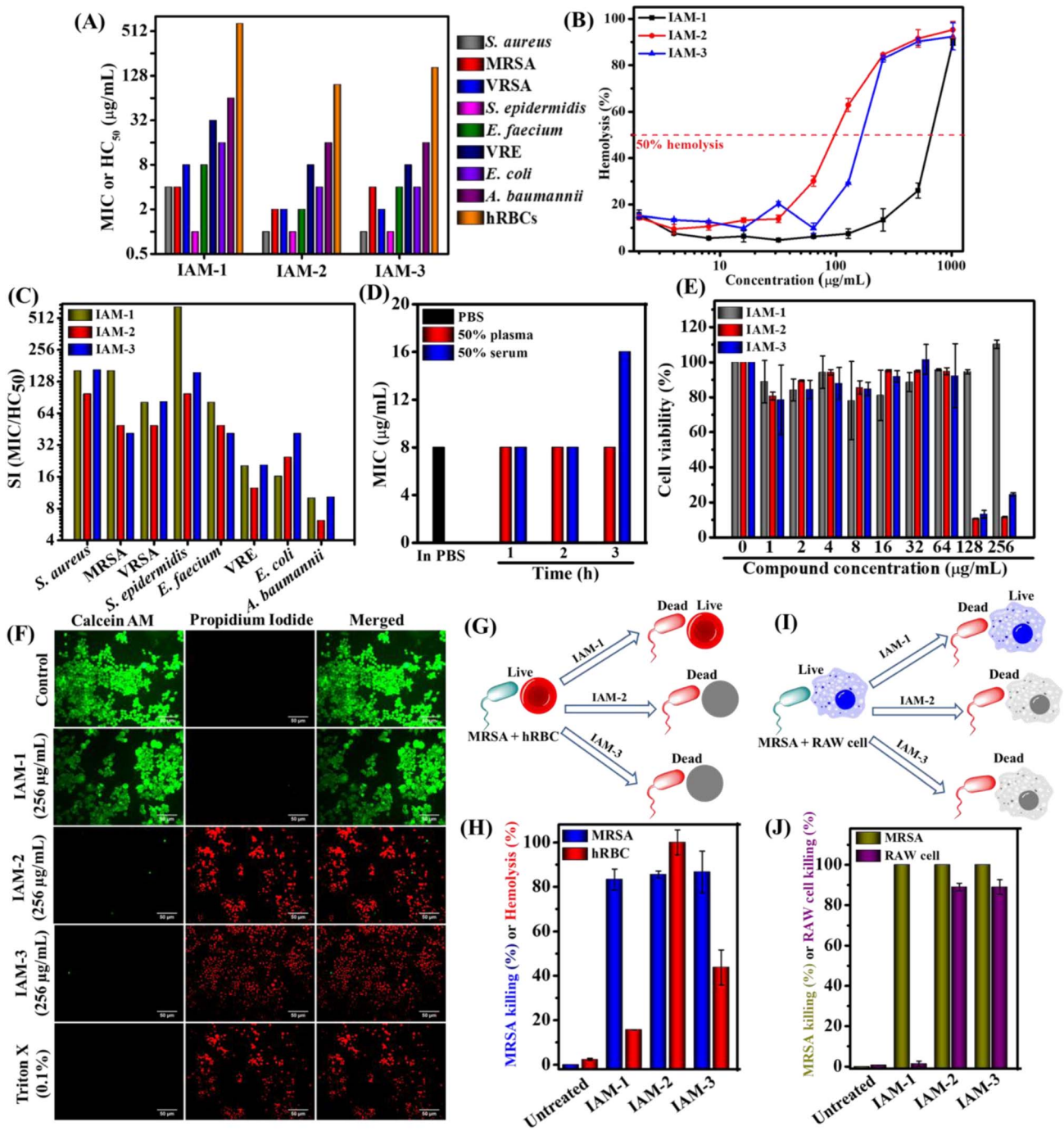

Fig. 2 (A) Antibacterial activity (MIC) and toxicity (HC_{50}) of IAMs: **1–3**. The experiment was performed twice in triplicate; (B) hemolysis percentage upon IAMs: **1–3** exposure at variable concentrations. The experiment was performed twice in triplicate; (C) selectivity index of IAMs: **1–3**. The SI values were calculated based on the average values of MIC and HC_{50}; (D) antibacterial activity of IAM-**1** against MRSA upon human blood plasma and serum pre-incubation at different time intervals (1 h, 2 h and 3 h). The experiment was conducted twice in triplicate; (E) RAW cell viability upon IAMs: **1–3** treatment; (F) fluorescence microscopy of RAW cells upon IAMs: **1–3** treatment at 256 μg mL^{-1} (257.8 μM); (G) schematic of a MRSA and hRBC co-culture study; (H) co-culture of MRSA and hRBC in the presence and absence of IAM-**1**, IAM-**2** and IAM-**3** at 256 μg mL^{-1} (257.8 μM); (I) schematic of a MRSA and RAW cell co-culture study and (J) co-culture of MRSA and RAW cells in the presence and absence of IAM-**1**, IAM-**2** and IAM-**3** at 256 μg mL^{-1} (257.8 μM). # MRSA: methylene resistant *S. aureus*, VRSA: vancomycin resistant *S. aureus* and VRE: vancomycin resistant *E. faecium*.

overall structure activity relationship (SAR), IAM-**1** was considered the optimized molecule for further investigation of its antibacterial efficacy in detail. Most importantly, IAM-**1**, IAM-**2**, and IAM-**3** were taken forward for the comparative studies on the role of positional isomerism in controlling selective interaction with bacteria over mammalian membranes.

Plasma and serum stability

Antibacterial compounds immune to instantaneous protease (present in blood plasma and serum) degradation unlike natural antimicrobial peptides (AMPs) have significant clinical relevance. Therefore, we evaluated the antibacterial activity (MIC) of the lead compound, IAM-**1** against MRSA upon pre-incubation with 50% human blood plasma and serum at different time intervals (1 h, 2 h, and 3 h) (Fig. 2D). Interestingly, the plasma pre-incubation led to no loss of antibacterial activity of IAM-**1**. Similarly, no changes in the MIC of IAM-**1** were observed upon 1 h and 2 h serum pre-incubations. However, 3 h serum pre-incubation of IAM-**1** resulted in a slight increase in its MIC by 2 fold (Fig. 2D). The result altogether demonstrated that this class of compound is relatively stable under complex blood components.

Cytotoxicity

Furthermore, the toxicity of the three positional isomers (IAMs: **1–3**) was evaluated by studying the cell viability against RAW cell lines through Alamar blue assay (Fig. 2E). The *ortho* isomer (IAM-**1**) showed 100% cell viability at 256 μg mL^{-1} (257.8 μM) after treating RAW cells for 24 h. However, *meta*-(IAM-**2**) and *para*-(IAM-**3**) exhibited 8% and 24% cell viability at 256 μg mL^{-1} (257.8 μM).

In addition to this study, fluorescence microscopy of RAW cells was performed upon IAMs **1–3** treatment by simultaneous staining with calcein-AM (stains live cells with green emission) and PI (stains cells with compromised cell membranes with red emission) (Fig. 2F). All the cells were found to be alive in the presence of IAM-**1** [256 μg mL^{-1} (257.8 μM)]. Nevertheless, almost no live cells were witnessed upon IAM-**2** (*meta*-isomer) and IAM-**3** (*para*-isomer) treatment at 256 μg mL^{-1} (257.8 μM). The overall results further ensured the superiority of the *ortho*-isomer over the *meta*- and *para*-isomers in terms of their detrimental effect on mammalian cells.

Co-culture study

To strengthen the impact of positional isomerism in achieving selective interaction, bacterial (MRSA) and mammalian cells (hRBCs or RAW cells) were treated with IAM **1–3** [256 mg mL^{-1} (257.8 μM)] under co-culture conditions instead of treating them individually[32] (Fig. 2F–I). A co-culture of MRSA and human erythrocytes (hRBCs) revealed 83% killing of MRSA and 16% lysis of hRBCs by the *ortho*-isomer, IAM-**1** (Fig. 2G and H). In contrast, the *meta*-isomer, IAM-**2** displayed 85% killing of MRSA and 100% lysis of hRBCs. Similarly, the *para*-isomer (IAM-**3**) exhibited 86% killing of MRSA and 44% lysis of hRBCs (Fig. 2G and H). On the other hand, 100% and 1.4% killing of MRSA and RAW cells, respectively, were observed upon 3 h of treatment with the *ortho*-isomer, IAM-**1** under co-culture conditions (Fig. 2I and J). In contrast, the *meta*- (IAM-**2**) and *para*-(IAM-**3**) isomers equally eliminated both MRSA (100% killing) and RAW cells (89% killing). However, the co-culture conditions did not affect the survival of both bacterial and mammalian cells in the absence of compound treatment in the case of untreated controls within the experimental time frame (15 min for hRBCs and 3 h for RAW cells). These results indicated that the *ortho*-isomer selectively killed bacteria over mammalian cells. However, *meta*- and *para*-isomers were equally detrimental to both bacteria and mammalian cells at the tested concentration. Overall, this result demonstrated the impact of positional isomerism in achieving selective antibacterial agents without altering the overall hydrophobicity of the molecular design.

Membrane leakage

The impact of positional isomerism on membrane perturbation was also studied by monitoring the leakage of carboxyfluorescein dye encapsulated within the liposomes made of DPPG : DPPE (88 : 12) and DPPC lipids mimicking bacterial and human erythrocyte model membranes, respectively (Fig. 3A–E). Specifically, carboxyfluorescein does not show significant emission when it is trapped within liposomes/vesicles, due to self-quenching effects at concentrations higher than 30 mM.[32] On the other hand, this particular dye displays a strong emission under diluted conditions (3 mM) when it releases from the vesicles upon interacting with an external membrane perturbing agent (Fig. 3A). Herein, dye-trapped vesicles were treated with IAMs **1–3** [160 μg mL^{-1} (161.1 μM)] (*ortho*-, *meta*- and *para*-isomers) at 50 s and the change in emission intensity maxima of carboxyfluorescein was monitored for 200 s (Fig. 3A). In the case of the bacterial model membrane, fluorescence intensity was enhanced upon treatment with all the positional isomers (IAMs **1–3**) indicating membrane leakage or membrane perturbation (Fig. 3B). More importantly, almost no enhancement in fluorescence intensity was observed upon the treatment of the mammalian model membrane with the *ortho*-isomer, IAM-**1**, indicating no significant membrane leakage (Fig. 3B).

In contrast, *meta*-(IAM-**2**) and *para*-(IAM-**2**) isomers displayed substantial enhancement in fluorescence intensity upon interacting with the mammalian model membrane (Fig. 3C). This suggested that *meta*- and *para*-isomers had a profound effect on the mammalian membrane along with the bacterial membrane. Furthermore, the rate constant of dye leakage was evaluated by fitting the data points of the emission spectrum [between compound addition (at 50 s) and triton-X addition (at 200 s)] using an exponential equation (Fig. S10†). Interestingly, the rate constant (k) of dye leakage was ~10 times higher in the case of the bacterial model membrane ($k = 1.9 \times 10^{-2}$ s^{-1}) compared to the mammalian model membrane ($k = 3 \times 10^{-3}$ s^{-1}) in the case of the *ortho*-isomer (IAM-**1**). However, the rate constant was of a similar magnitude for both bacterial and mammalian model membrane upon treatment with *meta*-[IAM-**2**; k (bacterial membrane): 1.9×10^{-2} s^{-1} and k (mammalian membrane): 1×10^{-2} s^{-1}] and *para*-[IAM-**3**; k(bacterial membrane): 3×10^{-2} s^{-1} and k (mammalian membrane): 0.8×10^{-2} s^{-1}] isomers. The results altogether established that the *ortho*-isomer was superior at the tested concentration in comparison to the *meta*- and *para*-isomers in achieving selective interaction with bacterial membranes over mammalian membranes.

Furthermore, to study the association of IAM-**1** with the mammalian and bacterial model phospholipid membranes

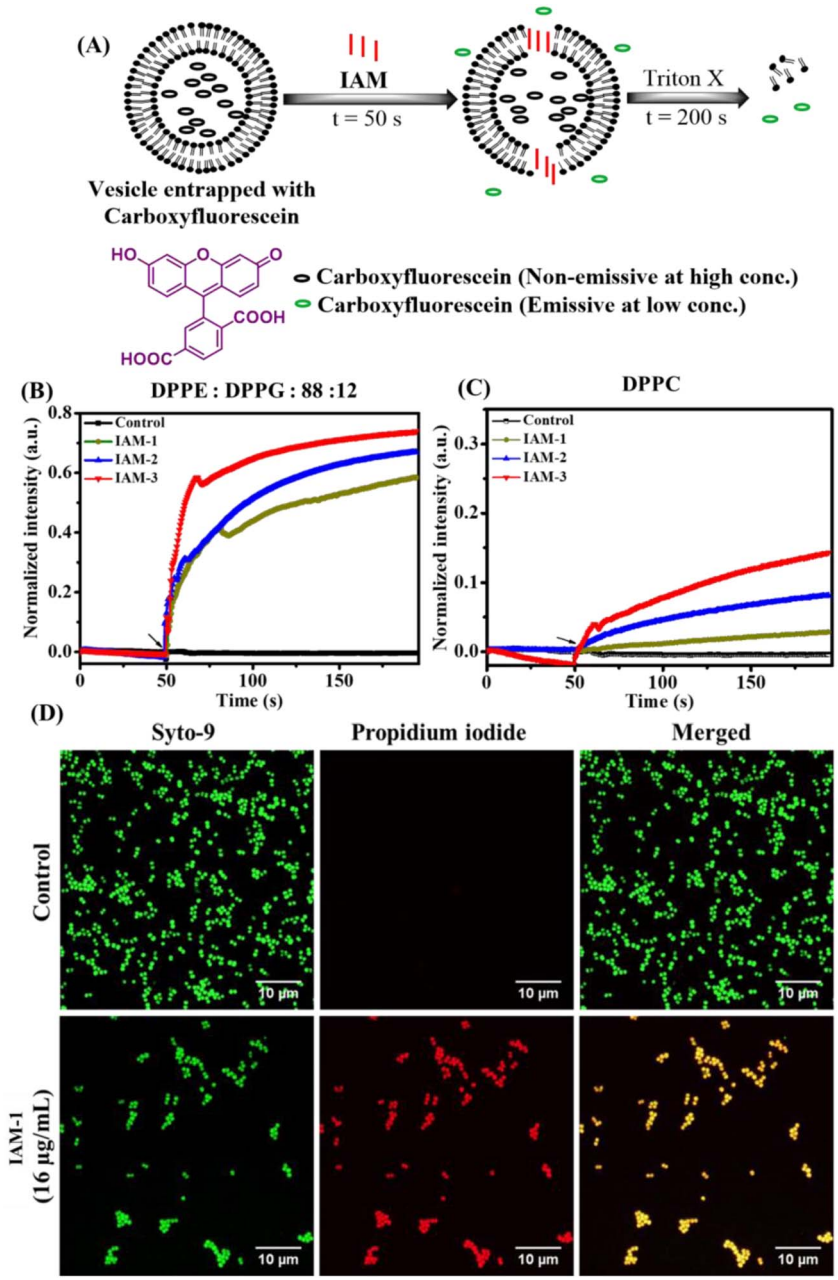

Fig. 3 (A) Schematic of a membrane leakage study using the carboxyfluorescein dye; (B) bacterial model membrane (DPPE : DPPG: 88 : 12) leakage upon treatment with IAMs: **1–3** at 160 μg mL^{-1} (161.1 μM); (C) mammalian model membrane (DPPC) leakage upon treatment with IAMs: **1–3** at 200 μg mL^{-1} (201.4 μM). The black arrows indicated the time of compound addition to the vesicles and (D) investigation on the antibacterial mechanism of action with the lead compound, IAM-**1**: through fluorescence microscopy of MRSA upon IAM-**1** treatment for 6 h.

composed of POPC and cholesterol (1 : 1) or POPE/POPG (7 : 3) respectively, the compound's absorbance and emission properties were exploited. The normalized absorbance and emission spectra of IAM-**1** in an aqueous solution are dominated by the dialkoxybenzene moiety, with only minor contributions by the phenylalanine residues (Fig. S11A†).[33] Herein, a fixed IAM concentration (10 μM) was titrated with increasing concentrations of vesicles. Membrane association caused an increase in fluorescence intensity, from which we could determine the fraction of membrane-bound compounds (Fig. S11B and S11C†). The water-membrane partition curves clearly show a much stronger affinity of IAM-**1** for liposomes mimicking the composition of bacterial membranes compared to the mammalian membrane. The anionic charge of POPG lipids definitely plays a role in the observed selectivity, but the negative intrinsic curvature of POPE and the effects of cholesterol on lipid packing likely contribute too.[34]

Furthermore, the influence of positional isomerism was established also by studying the change in membrane fluidity/dynamics upon compound treatment by encapsulating laurdan dye (6-dodecanoyl-2-dimethylaminonaphthalene) inside bacterial and mammalian model membranes (ESI Figure S12†).[30,31]

Membrane active mechanisms

The biophysical investigation on membrane fluidity and membrane leakage as described previously indicated the membrane active nature of isoamphipathic antibacterial molecules. However, the detailed membrane activity of the lead *ortho*-isomer (IAM-**1**) was further investigated by performing membrane depolarization and outer membrane permeabilization against MRSA and *E. coli* respectively (Fig. S13A and S13B†). The membrane active nature was further supported by studying fluorescence microscopic analysis of bacteria upon IAM-**1** treatment (Fig. 3D). Finally, the interaction of the compound with bacterial membranes was investigated through a theoretical study using the minimum bias approach (Fig. 4A and B).

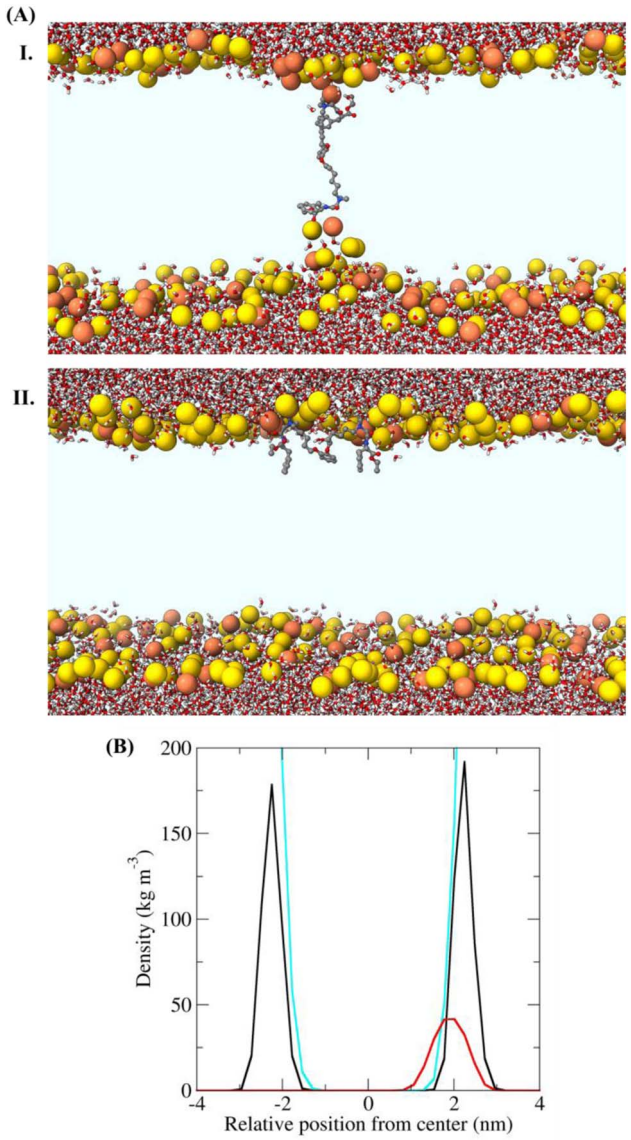

Fig. 4 (A) Structures of the bacterial membrane in the three simulations in which a defect free bilayer was formed. Water molecules and IAM-**1** are shown in stick representation and coloured according to atom type (C = grey, O = red, N = blue, and H = white). The phosphorus atoms of the lipids are shown as yellow or orange spheres (for POPE and POPG, respectively). (I) Transmembrane orientation and (II) superficial orientation of IAM-**1** in the lipid bilayer. The other parts of the lipid molecules are not shown, for the sake of clarity, so that the light blue area corresponds to the hydrophobic core of the bilayer. (C) Density of selected groups in the equilibrated trajectory (last 20 ns, after the annealing process), showing the different depth of insertion of the analogue. The colour code used in the structural figures is the same as that in Fig. 4B and water is not shown, for the sake of clarity. In the bottom panel the density is shown in black for P atoms, in cyan for water and in red for IAM-**1** respectively.

Membrane depolarization

Membrane-potential sensitive dye 3,3′-dipropylthiadicarbocyanine iodide [DiSC3 (5)] was selected for this study. Under normal potential across the membrane, DiSC3 (5) dye distributes inside and outside the bacterial envelope. Thereby, the fluorescence intensity of the dye decreases, due to its self-quenching inside the bacterial cells. Treatment with compounds which affect the normal membrane potential results in the release of the dye in the external media, leading to an increase in fluorescence intensity.[27] Due to the addition of various concentrations of IAM-**1** [16 μg mL^{-1} (16.1 μM) and 32 μg mL^{-1} (32.2 μM)] an increment in fluorescence intensity was observed for both *S. aureus* and *E. coli* (Fig. S13A†). The extent of fluorescence enhancement followed a concentration dependence (greater effect at higher concentrations of the compound). This observation clearly indicated the perturbation of normal membrane potential by this class of molecules.

Outer membrane (OM) permeabilization

Since the outer membrane (OM) of Gram-negative bacteria serves as a diffusion barrier for multiple antibiotics, the OM permeabilization of IAM-**1** was investigated against *E. coli* using hydrophobic dye *N*-phenyl naphthylamine (NPN). This particular dye emits upon binding to the hydrophobic region of the bacterial outer membrane when an external membrane active agent perturbs it.[27] Herein, NPN fluorescence intensity was observed to be enhanced upon treatment with IAM-**1** at different concentrations [32 μg mL^{-1} (32.2 μM) and 64 μg mL^{-1} (64.4 μM)] (Fig. S13B†). The extent of fluorescence enhancement followed a concentration dependence (greater effect at higher concentrations of the compound). These results confirmed the outer membrane perturbation ability of the compound in a dose-dependent mode.

Fluorescence microscopy

The membrane active nature of IAM-**1** was further confirmed by performing fluorescence microscopy of MRSA by concomitant staining with Syto-9 and PI (Fig. 3D). In the case of the untreated control, all the MRSA cells were alive since they were solely stained with green emissive Syto-9 dye. Importantly, IAM-**1** [16 μg mL^{-1} (16.1 μM)] treated MRSA cells were equally stained with both green emissive Syto-9 and red emissive PI and the merged image showed a co-localization of both dyes. This result indicated that the bacterial cell membranes were compromised upon compound treatment and re-established the membrane active nature of IAM-**1**.

Molecular dynamics simulations

To further support the membrane active nature, we performed simulations of the lead compound, IAM-**1** in the presence of POPE/POPG lipids, using the so-called "minimum-bias" approach, where simulations start from a random mixture of bioactive molecules, lipids, and water. With this approach, the bilayer self-assembles, and the system is initially very fluid. This method can individuate the positions and orientations of the molecule that correspond to free energy minima.[35] Since our goal was to determine the position, orientation, and conformation of the IAM in the membrane-bound state, we simulated conditions under which pore formation was not expected (IAM-**1**/lipid = 1/128). Three independent simulations were performed for IAM-**1**. A defect-free bilayer formed during the simulation time only in two cases. Representative structures at the ends of these trajectories are reported in Fig. 4A. IAM-**1** populated both a superficial and a transmembrane orientation. IAM-**1** inserted below the head groups when surface bound. It adopted an M-shaped conformation, with the phenyl and alkoxybenzene groups pointing towards the hydrophobic core of the bilayer and the cationic amino groups interacting with the phosphates of the lipids (Fig. 4B). The structure of the IAM-**1** inserted in the transmembrane orientation shows that this molecule cannot reach easily from one side to the other of the membrane. In the final part of the trajectory, the distance between the two N atoms of the charged amino groups was on average 1.8 nm, *i.e.*, less than the normal thickness of the bilayer (approximately 4 nm). As a consequence, a local thinning of the membrane was observed.

Overall, these data suggest that the IAM molecules might act similarly to antimicrobial peptides, by binding to the membrane surface, below the head groups, and thus inducing stress in the surface tension of the outer lipid leaflet.[34,35] This stress, in turn, can lead to IAM insertion in a transmembrane orientation and/or to membrane leakage or membrane perturbation.

Time-kill kinetics

To understand the antibacterial action window, bactericidal kinetics studies of the lead compound, IAM-**1** were performed against planktonic MRSA and *E. coli* (Fig. 5A and B). IAM-**1** at 16 μg mL^{-1} (16.1 μM) reduced 2 log of MRSA and *E. coli* respectively at 12 h. Importantly, at a higher concentration of 32 μg mL^{-1} (32.2 μM) both MRSA and *E. coli* were completely (5–6 log reduction) eliminated by IAM-**1** at 12 h. These observations suggested that the lead *ortho*-isomer displayed relatively delayed bactericidal kinetics in a dosage dependent manner.

Activity against metabolically inactive bacteria

Parallel with antimicrobial resistance, the predominance of metabolically inactive bacterial sub-population in chronic infections is another major challenge to global public health.[36,37] Stationary and persister phase bacterial species belong to these metabolically inactive dormant sub-classes. Most of the conventional antibiotic therapeutics are ineffective against dormant bacteria since they almost shut down most of their biological processes (*e.g.* cell division, protein synthesis, DNA replication, *etc.*), a specific target of the antibiotics. Hence, the anti-stationary and anti-persister activity of the lead *ortho*-isomer (IAM-**1**) was investigated as depicted in Fig. 5C–F. For instance, IAM-**1** at both 16 μg mL^{-1} (16.1 μM) and 32 μg mL^{-1} (32.2 μM) completely (6log reduction) eradicated stationary cells of MRSA (Fig. 5C). Similarly, at a lower concentration of 32 μg mL^{-1} (32.2 μM), IAM-**1** showed 2.2 log reduction of stationary cells of *E. coli.* Noticeably, complete elimination of *E.coli* stationary cells was observed at a twofold higher concentration of 64 μg mL^{-1} (64.4 μM) (Fig. 5D). Alongside, IAM-**1** killed the persister cells of *S. aureus* completely (6 log reduction) at both 16 μg mL^{-1} (16.1 μM) and 32 μg mL^{-1} (32.2 μM) (Fig. 5E). Likewise, the compound displayed 2 log reduction of *E. coli* persister cells at 32 μg mL^{-1} (32.2 μM). Moreover, the compound was efficacious in the complete elimination of *E. coli* persister cells at 64.4 μM (Fig. 5F). However, the widely prescribed antibiotic for Gram-positive infection, vancomycin [64 μg mL^{-1} (64.4 μM)] displayed negligible reduction (0.5–1 log reduction) of stationary and persister cells of MRSA and *S. aureus*. On the other hand, colistin, a widely used antibiotic for Gram-negative infection, [32 μg mL^{-1} (27.7 μM)] displayed 2 log and 3 log reduction of stationary and persister cells of *E. coli* respectively. Taken together, these data demonstrated that the lead isoamphipathic antibacterial molecule (IAM-**1**) was competent enough to combat dormant bacteria, one of the critical factors behind chronic and recurrent infections. Remarkably, this class of antibacterial molecules is way better than conventional antibiotics at tackling dormant bacterial sub-populations.

Anti-biofilm efficacy

An escalation tendency of biofilm formation by multidrug-resistant bacteria is one of the emerging problems within the hurdles of antimicrobial resistance.[5,6,38,39] Almost 80% of the infections are in conjunction with biofilm formation.

The abundance of thick extracellular polymeric matrices accompanied by dormant bacterial sub-populations in the biofilm renders conventional antibiotics ineffective. Hence, antimicrobials with potent anti-biofilm efficacy are in high demand. Towards this aim, the biofilm disruption efficacy of IAM-**1** was investigated through crystal violet (CV) staining and bacterial cell viability counting (Fig. 5G and H). IAM-**1** displayed ~70% reduction in the MRSA biofilm biomass at 128 μg mL^{-1} (128.9 μM) (32 × MIC) in CV staining (Fig. 5G). Positively charged IAM-1 interacts with various negatively charged components of extracellular polymeric matrices of the biofilm and hydrophobicity of the compound aids in biofilm disruption. However, 30% reduction in biofilm biomass was observed upon vancomycin treatment at its 64 times MIC [64 μg mL^{-1} (64.4 μM)]. Additionally, bacterial cell viability assay was performed to understand whether the biofilm-embedded MRSA was killed by the compound along with biofilm disruption. IAM-**1** at 128 μg mL^{-1} (128.9 μM) killed 3.5 log of biofilm-trapped MRSA whereas vancomycin at 64 μg mL^{-1} (44.2 μM) was

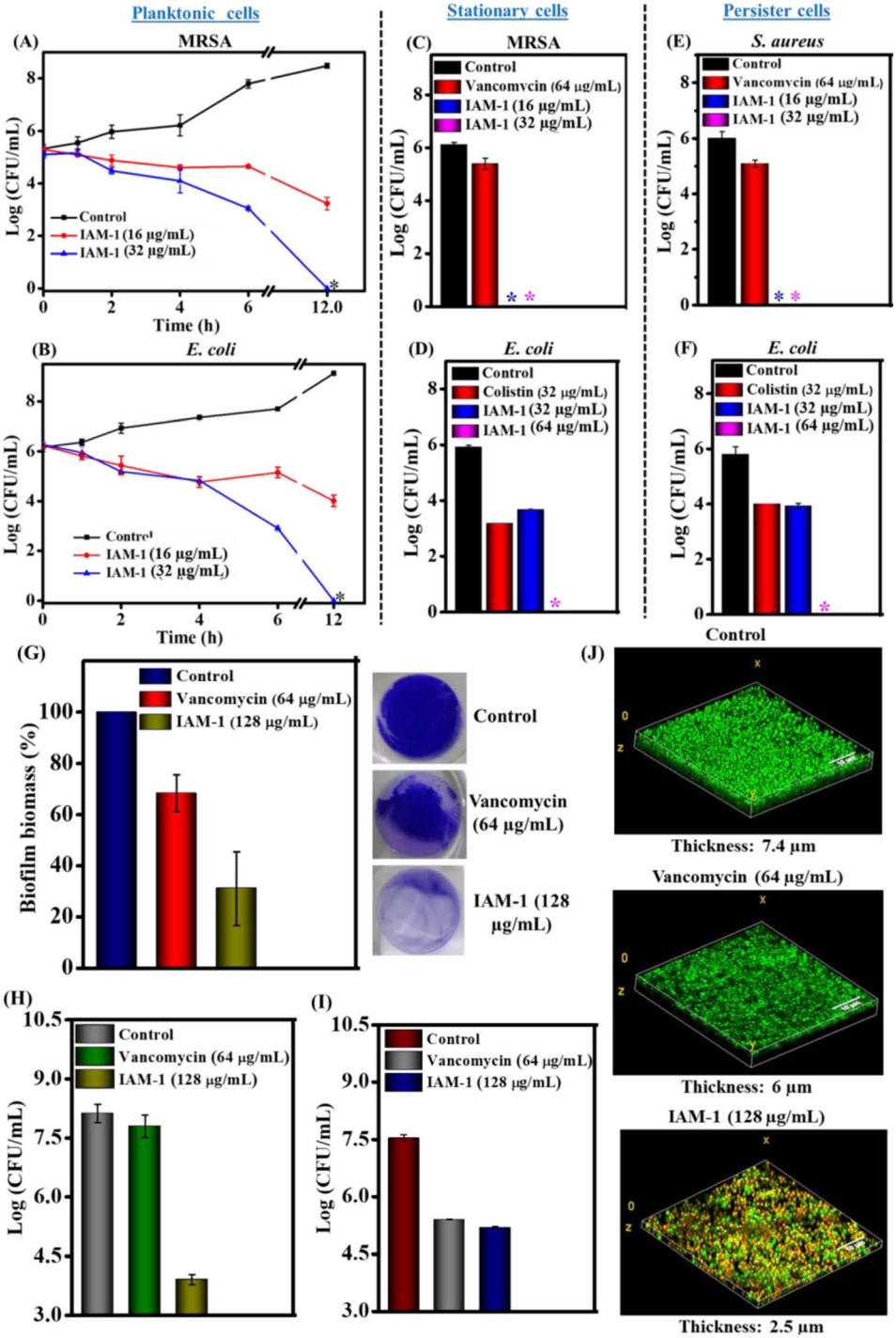

Fig. 5 Bactericidal kinetics of IAM-**1** against planktonic (A) MRSA ATCC 33591 and (B) *E. coli* MTCC 443; anti-stationary phase activity of IAM-**1** (upon 6 h treatment) against stationary cells of (C) MRSA ATCC 33591 and (D) *E. coli* MTCC 443; anti-persister phase activity of IAM-**1** against persister cells of (E) *S. aureus* MTCC 737 and (F) *E. coli* MTCC 443. The asterisk (*) corresponds to < 50 CFU. MRSA biofilm disruption upon IAM-**1** treatment: (G) crystal violet staining of MRSA ATCC 33591 biofilm; (H) biofilm-embedded MRSA ATCC 33591 cell viability; (I) biofilm-dispersed MRSA cell viability and (J) fluorescence microscopy of MRSA ATCC 33591 biofilm disruption. The live/dead ratio; control: 96% : 4%, vancomycin [64 μg mL^{-1} (44.2 μM)]: 80% : 20% and IAM-**1** [128 μg mL^{-1} (128.9 μM)]: 15% : 75%. The live/dead ratio was calculated using image J.

completely ineffective in eliminating MRSA in the biofilm (Fig. 5H). Furthermore, the efficacy of the compound against biofilm-dispersed bacterial cells was investigated. IAM-1 (128.9 μM) displayed 2.3 log reduction (99.5%) of bacterial burden originating from biofilm dispersion (Fig. 5I). In addition, biofilm disruption was visualized through fluorescence microscopy by dual staining with Syto-9 (stains both live and dead cells with green emission) and PI (stains membrane compromised

bacterial cells with red emission). Treatment with IAM-**1** at 128 μg mL^{-1} (128.9 μM) drastically reduced the thickness of the MRSA biofilm to 2.5 μm while the untreated biofilm displayed a thickness of 7.4 μm (Fig. 5J). Along with the thickness reduction, the compound was competent to kill biofilm-embedded MRSA ensured by the presence of a large fraction of MRSA (75% dead) with yellow staining (due to colocalization of green and red colours). In contrast, upon vancomycin [64 μg mL^{-1} (44.2 μM) treatment, the biofilm showed green emission (80% live MRSA) with a thickness of 6 μm. In this context, we hypothesize that probably the interaction between positively charged IAM-**1** and various negatively charged components of extracellular polymeric matrices of the biofilm is responsible for biofilm disruption. Additionally, efficacy against dormant bacterial sub-population can be held accountable for the killing of biofilm-embedded MRSA by IAM-**1**. These overall results suggested that the lead *ortho*-isomer, IAM-**1** was a promising candidate with a potent biofilm disruption efficacy.

Dermal toxicity

The therapeutic application of the lead compound requires toxicological evaluation in animal models as a part of pre-clinical studies. Therefore, the dermal toxicity of IAM-**1** was evaluated upon its topical application at 200 mg kg^{-1} to the dermal layers in the dorsal area of the mice. The effect of the compound on the mice's skin surface was monitored visually for 14 days. We did not observe any significant side effects (such as convulsions, tremors, salivation, irritation, *etc.*) of the compound on the mice. Furthermore, the histopathological changes were investigated through hematoxylin and eosin staining of both saline treated and compound treated dermal tissues (Fig. 6A). The saline treated dermis showed the normal appearance of an epidermis layer lined with stratified squamous epithelial cells and covered by keratin layers (arrow). The dermis contained the sweat and sebaceous glands (SGs), hair follicles (HFs), adipose tissue, and muscle layer (M). The dermis also showed the presence of a spindle-shaped fibrous connective layer with an oval-shaped nucleus (asterisk). The compound treatment also led to a similar observation on day 7 and day 14 (Fig. 6A). These results suggested the non-toxic nature of the compound in the animal model and revealed its suitability for *in vivo* topical application.

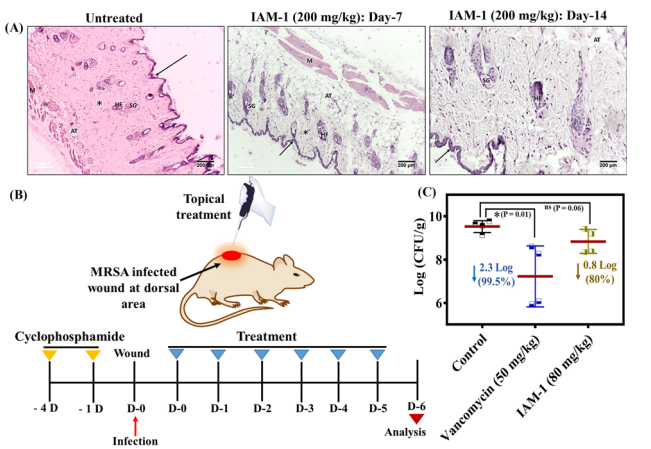

Fig. 6 (A) Histopathology (H and E staining) of untreated and IAM-**1** (200 mg kg^{-1}) treated mouse dermal tissue; wound infection with MRSA, (B) experimental plan and (C) experimental outcome. Values are presented as mean ± standard deviation for a group of 4 mice. Statistical analysis was conducted using GraphPad Prism 7 through an unpaired student-*t* test and $P < 0.05$ was considered statistically significant.

In vivo antibacterial activity

Furthermore, the antibacterial efficacy of IAM-**1** was evaluated in a murine model of dermal wound infection against MRSA. A wound was created using a scalpel in the dorsal area of neutropenic mice after fur removal and the wound was infected with 10^7 CFU mL^{-1} inoculation of MRSA. Four hours post-infection, the wound was treated topically with 80 mg kg^{-1} (below the tolerable dosage of dermal administration) IAM-**1**, and 50 mg kg^{-1} vancomycin treatment was also initiated as a positive control. The same dosages of treatments (OD: once a day) were continued with vancomycin and compound for 5 consecutive days (Fig. 6B). Furthermore, bacterial cell viability assay within the infected dermal tissues was conducted on the 6th day. The results demonstrated a 2.3 log reduction (99.5%) of MRSA burden by vancomycin (Fig. 6C). Similarly, IAM-**1** displayed an 80% reduction in MRSA burden compared to the untreated control (Fig. 6C).

Conclusion

A new class of amino acid based isoamphipathic antibacterial molecules has been developed and they showed appreciable antibacterial activity against various Gram-positive and Gram-negative bacteria including multi-drug resistant clinical isolates. More importantly, apart from hydrophobicity modulation in controlling antibacterial activity and toxicity, positional isomerism has been recognized as an influential factor in the design. Co-culture studies, investigation on membrane dynamics through molecular dynamics (MD) simulations and membrane leakage and membrane fluidity studies established the superiority of the *ortho*-isomer (IAM-**1**) in achieving selective interaction with bacterial membranes over mammalian membranes in comparison to *meta*-(IAM-**2**) and *para*-(IAM-**3**) isomers owing to its local membrane thinning effect. MD simulation, biophysical and spectroscopic studies also revealed that this class of compound primarily targets bacterial membranes through different modes of action such as trans-membrane orientation, membrane leakages or perturbation *etc.* Moreover, the potency to combat metabolically inactive bacterial sub-population and bacterial biofilms made the *ortho*-isomer a promising candidate to encounter chronic infections. The lead isomer displayed moderate *in vivo* antibacterial activity in a murine model of wound infection against MRSA with no notable *in vivo* dermal toxicity. Altogether, the current article explored a new guiding parameter for achieving a selective antibacterial agent.

Ethical statement

The antibacterial studies including hemolytic activity were conducted as per the approval of the Institutional Bio-safety Committee of the Jawaharlal Nehru Centre for Advanced Scientific Research (JNC/IBSC/2020/JH–12). The *in vivo* animal studies were executed according to the protocols sanctioned by the Institutional Animal Ethics Committee (IAEC) of the Jawaharlal Nehru Centre for Advanced Scientific Research (JNCASR) (201/Go/ReBi/S/2000/CPCSEA).

Data availability

The synthetic protocols for IAMs, molecular characterization, experimental protocols for biological, biophysical, and animal studies, and theoretical studies can be found in the ESI.†

Author contributions

The work and the experiments were designed by S. B. and J. H. The theoretical studies were designed, performed, and analyzed by A. G., P. C., G. B., and L. S. Cell toxicity assay was performed by B. B. All other studies were conducted by S. B., S. M., L. J, and D. B. All the data were analyzed by S. B., S. M., and J. H. The membrane leakage results were analyzed by D. B., S. B. and J. H. The water partition to membrane study was conducted and analyzed by C. T. and L. S. The manuscript was written by S. B., J. H., and L. S. All the authors approved the final version of the manuscript.

Conflicts of interest

The authors declare no conflicts of interest.

Acknowledgements

We thank Prof. C. N. R. Rao (JNCASR) for his constant support and encouragement. J. H. acknowledges JNCASR, IFCPAR (IFC/62T10-1), and DBT (BT/PR/31801/MED/29/1394/2019). We thank Dr Subi J. George for helping with the instrumental facility for the membrane leakage study. This project was also supported by a PRIN2020 grant (2020833Y75) by the Italian Ministry of University and Research (to LS). The authors are grateful to CINECA for providing computational resources. Mr Francesco Riccitelli is acknowledged for his assistance with water-membrane partition experiments. We thank Dr Sreyan Ghosh for helping with the *in vivo* experiments. We acknowledge Rohana Veterinary Diagnostic laboratory (Bangalore, Karnataka, India) for their assistance in *in vivo* studies.

References

1 K. Bush, P. Courvalin, G. Dantas, J. Davies, B. Eisenstein, P. Huovinen, G. A. Jacoby, R. Kishony, B. Kreiswirth, E. Kutter, et al., *Nat. Rev. Microbiol.*, 2011, **9**, 894–896.
2 H. W. Boucher, G. H. Talbot, J. S. Bradley, J. E. Edwards, D. Gilbert, L. B. Rice, M. Scheld, B. Spellberg and J. Bartlett, *Clin. Infect. Dis.*, 2009, **48**, 1–12.
3 R. Laxminarayan, A. Duse, C. Wattal, A. K. M. Zaidi, H. F. L. Wertheim, N. Sumpradit, E. Vlieghe, G. L. Hara, I. M. Gould, H. Goossens, et al., *Lancet Infect. Dis.*, 2013, **13**, 1057–1098.
4 D. Davies, *Nat. Rev. Drug Discovery*, 2003, **2**, 114–122.
5 J. W. Costerton, P. S. Stewart and E. P. Greenberg, *Science*, 1999, **284**, 1318–1322.
6 P. S. Stewart and J. W. Costerton, *Lancet*, 2001, **358**, 135–138.
7 K. E. Watkins and M. Unnikrishnan, *Adv. Appl. Microbiol.*, 2020, **112**, 105–141.
8 G. Taubes, *Science*, 2008, **321**, 356–361.
9 U. Theuretzbacher, S. Gottwalt, P. Beyer, M. Butler, L. Czaplewski, C. Lienhardt, L. Moja, M. Paul, S. Paulin, J. H. Rex, et al., *Lancet Infect. Dis.*, 2019, **19**, e40–e50.
10 U. Theuretzbacher, K. Outterson, A. Engel and A. Karlén, *Nat. Rev. Microbiol.*, 2020, **18**, 275–285.
11 E. Tacconelli, E. Carrara, A. Savoldi, S. Harbarth, M. Mendelson, D. L. Monnet, C. Pulcini, G. Kahlmeter, J. Kluytmans, Y. Carmeli, et al., *Lancet Infect. Dis.*, 2018, **18**, 318–327.
12 D. E. Bloom and D. Cadarette, *Front. Immunol.*, 2019, **10**, 549.
13 M. S. Ganewatta and C. Tang, *Polymer*, 2015, **63**, A1–A29.
14 M. M. Konai, B. Bhattacharjee, S. Ghosh and J. Haldar, *Biomacromolecules*, 2018, **19**, 1888–1917.
15 C. Ghosh and J. Haldar, *ChemMedChem*, 2015, **10**, 1606–1624.
16 E. F. Palermo, K. Lienkamp, E. R. Gillies and P. J. Ragogna, *Angew. Chem.*, 2019, **58**, 2–6.
17 A. Cisse, A. Marquette, M. Altangerel, J. Peters and B. Bechinger, *J. Phys. Chem. B*, 2021, **125**, 10213–10223.
18 G. N. Tew, R. W. Scott, M. L. Klein and W. F. Degrado, *Acc. Chem. Res.*, 2010, **43**, 30–39.
19 I. S. Radzishevsky, S. Rotem, D. Bourdetsky, S. Navon-Venezia, Y. Carmeli and A. Mor, *Nat. Biotechnol.*, 2007, **25**, 657–659.
20 Y. Niu, S. Padhee, H. Wu, G. Bai, Q. Qiao, Y. Hu, L. Harrington, W. N. Burda, L. N. Shaw, C. Cao, *et al.*, *J. Med. Chem.*, 2012, **55**, 4003–4009.
21 W. Chin, G. Zhong, Q. Pu, C. Yang, W. Lou, P. F. De Sessions, B. Periaswamy, A. Lee, Z. C. Liang, X. Ding, *et al.*, *Nat. Commun.*, 2018, **9**, 917.
22 J. S. Brown, Z. J. Mohamed, C. M. Artim, D. N. Thornlow, J. F. Hassler, V. P. Rigoglioso, S. Daniel and C. A. Alabi, *Commun. Biol.*, 2018, **1**, 220.
23 C. Ghosh, G. B. Manjunath, P. Akkapeddi, V. Yarlagadda, J. Hoque, D. S. S. Uppu, M. M. Konai and J. Haldar, *J. Med. Chem.*, 2014, **57**, 1428–1436.
24 D. S. S. M. Uppu, P. Akkapeddi, G. B. Manjunath, V. Yarlagadda and J. H. J. Haldar, *Chem. Commun.*, 2013, **49**, 9389–9391.
25 C. Ghosh, P. Sarkar, S. Samaddar, D. S. S. M. Uppu and J. Haldar, *Chem. Commun.*, 2017, **53**, 8427–8430.
26 S. Barman, G. Dhanda, P. Naik, R. Mukherjee, L. Jolly, J. Joseph and J. Haldar, *Adv. Ther.*, 2022, **5**, 2100234.

27 S. Barman, M. M. Konai, S. Samaddar and J. Haldar, *ACS Appl. Mater. Interfaces*, 2019, **11**, 33559–33572.
28 M. Zasloff, *Nature*, 2002, **415**, 389–395.
29 R. E. W. Hancock and H. G. Sahl, *Nat. Biotechnol.*, 2006, **24**, 1551–1557.
30 S. A. Sanchez, M. A. Tricerri and E. Gratton, *Proc. Natl. Acad. Sci. U. S. A.*, 2012, **109**, 7314–7319.
31 D. S. S. M. Uppu, M. M. Konai, U. Baul, P. Singh, T. K. Siersma, S. Samaddar, S. Vemparala, L. W. Hamoen, C. Narayana and J. Haldar, *Chem. Sci.*, 2016, **7**, 4613–4623.
32 F. Savini, V. Luca, A. Bocedi, R. Massoud, Y. Park, M. L. Mangoni and L. Stella, *ACS Chem. Biol.*, 2016, **12**, 52–56.
33 *Handbook of Chemistry and Physics*, ed. R. C. Weast, CRC Press Inc., Boca Raton, Florida, 60th edn, 1979, p. C-161.
34 S. Bobone and L. Stella, *Adv. Exp. Med. Biol.*, 2019, **1117**, 175–214.
35 A. Farrotti, G. Bocchinfuso, A. Palleschi, N. Rosato, E. S. Salnikov, N. Voievoda and B. B. L. Stella, *Biochim. Biophys. Acta*, 2015, **1848**, 581–592.
36 K. Lewis, *Nat. Rev. Microbiol.*, 2007, **5**, 48–56.
37 J. Jaishankar and P. Srivastava, *Front. Microbiol.*, 2017, **8**, 2000.
38 L. Hall-Stoodley, J. W. Costerton and P. Stoodley, *Nat. Rev. Microbiol.*, 2004, **2**, 95–108.
39 P. S. Stewart, *Int. J. Med. Microbiol.*, 2002, **292**, 107–113.
40 K. G. Varnava, A. S. Mohid, P. Calligari, L. Stella, J. Reynisson, A. Bhunia and V. Sarojini, *Bioconjugate Chem.*, 2019, **30**, 1998–2010.

Supporting Information

Isoamphipathic Antibacterial Molecule Regulating Activity and Toxicity through Positional Isomerism

Swagatam Barman,[a] Sudip Mukherjee,[a] Logia Jolly,[a] Cassandra Troiano,[b] Alessandro Grottesi,[c] Debajyoti Basak,[a] Paolo Calligari,[b] Brinta Bhattacharjee,[a] Gianfranco Bocchinfuso,[b] Lorenzo Stella,[b] and Jayanta Haldar*[a,d]

[a] Antibacterial Research Laboratory, New Chemistry Unit, Jawaharlal Nehru Centre for Advanced Scientific Research (JNCASR), Jakkur, Bangalore, India-560064. E-mail: jayanta@jncasr.ac.in.

[b] Department of Chemical Science and Technologies, University of Rome Tor Vergata, via della Ricerca Scientifica, 1; 00133, Rome, Italy.

[C]Cineca, Via dei Tizii, 6; 00185, Rome, Italy

[d] School of Advanced Materials, Jawaharlal Nehru Centre for Advanced Scientific Research (JNCASR), Jakkur, Bangalore, India-560064

Table of Contents:

Experimental Section

Materials and instrumentations. Dichloromethane, ethanol, thionyl chloride was obtained from Spectrochem (India) and all the solvents were of reagent grade and dried before use according to the requirement. Bromoacetyl bromide, 1,4-dibromohexane, 1,6-dibromooctane, 1,10-dibromodecane, catechol, hydroquinone, resorcinol, *N*-phenyl naphthylamine, propidium iodide, 3, 3′-dipropylthiadicarbocyanine iodide [$DiSC_3$ (5)], DPPE, DPPG, DPPC, 5(6)-carboxyfluorescein, laurdan dye were procured from Sigma-Aldrich. L-Phenylalanine was obtained from Spectrochem (India). Analytical thin layer chromatography (TLC) was performed on silica gel 60 F254 percolated E. Merck TLC plates and visualized by using iodine or ninhydrin. Cholesterol, POPC, POPG and POPE were purchased from Avanti Polar Lipids (Birmingham, AL, USA) with a purity >99%. Bruker AMX-400 spectrometer was used to record nuclear magnetic resonance (NMR) spectra in deuterated solvents. 6538-UHD Accurate Mass Q-TOF LC-MS instrument was used to record mass spectra. Tecan Infinite M200 PRO Microplate Reader was used for optical density (O.D.) measurement. UV-visible experiments were performed on a Jasco V-770 spectrophotometer. Fluorescence measurements for the biophysical investigations were carried out using Jasco FP-8500 spectrofluorimeter. Bacterial strains, *S. aureus* MTCC737, *E. coli* MTCC443, *A. baumannii* MTCC1425 were procured from MTCC (Chandigarh, India). VRE 909 and VRSA 4 were obtained from Anthem Bioscience (Bangalore, India). MRSA ATCC33591, *E. faecium* ATCC19634, and *K. pneumoniae* ATCC700603 were purchased from ATCC (Rockville, MD, USA). *S. aureus*, *E. coli*, MRSA, *K. pneumoniae* and *A. baumannii* were grown in Mueller Hinton Broth (MHB-HIMEDIA-M391). Brain heart infusion broth (BHI) was to inoculate *E. faecium* and VER. MacConkey Agar and Nutrient agar were used as a solid media for Gram-negative and gram-positive bacteria. 96 well plates, 6 well plates and transparent black 96 well plates were obtained from Vasa Scientific (Bangalore, India).

Synthesis and characterization

Synthetic protocol of dibromohexyloxy benzene (1a, 2a and 3a). Aromatic diol (catechol / resorcinol / hydroquinone) (2.5 g, 22.7 mmol), *N*, *N*′-hexyl dibromide (10.5 mL, 68 mmol) and potassium carbonate (14.2 g, 102.7 mmol) were taken together in a RB and refluxed at 60 ˚C in 50 mL acetone under argon atmosphere for 24 h. After cooling the reaction mixture to the room temperature, the solid potassium carbonate was removed using Whatman 40 filter paper. Afterward, acetone was evaporated using rota evaporator and the solid residue was dissolved in 50 mL ethyl acetate. Next, the crude product containing ethyl acetate layer was washed thrice with distilled water and passed over anhydrous Na_2SO_4. Finally, the crude product was purified through column chromatography (stationary phase: silica gel, Eluent: hexane and ethyl acetate). The final product appeared as white solid with 60-65% yield.

1,2-bis((6-bromohexyl)oxy)benzene (1a). Yield 65%; ^{1}H-NMR (400 MHz, $CDCl_3$): δ/ppm. 1.50-1.91 (m, -$OCH_2(CH_2)_4CH_2Br$, 16H), 3.42 (t, *J* = 6.8 Hz, -$OCH_2(CH_2)_2CH_2Br$, 4H), 4.0 (t, *J* =

6.5 Hz, -OCH_2(CH_2)$_2$$CH_2$Br, 4H), 6.88 (s, -$H_{Ar}$, 4H). HRMS (m/z): 435.0520, 437.0499 [(M+H)$^+$] (observed), 435.0529, 437.0508 [(M+H)$^+$] (calculated).

1,3-bis((6-bromohexyl)oxy)benzene (2a). Yield 64%; ^{1}H-NMR (400 MHz, $CDCl_3$): δ/ppm. 1.49-1.51 (m, -O(CH_2)$_2$(CH_2)$_2$(CH_2)$_2$Br, 8H), 1.77-1.80 (m, -O(CH_2)$_4$C$H_2$$CH_2$Br, 4H), 1.86-1.91 (m, -OCH_2CH_2(CH_2)$_4$Br, 4H), 3.42(t, *J* = 6.8 Hz, -O(CH_2)$_4$$CH_2CH_2$Br, 4H), 3.92-3.94 (t, *J* = 6.4 Hz, -OC$H_2$$CH_2$($CH_2$)$_4$Br, 4H), 6.44-6.49 (m, -$H_{Ar}$, 3H), 7.15 (t, *J* = 8.2 Hz, -H_{Ar}, 1H). HRMS (m/z): 435.0520, 437.0499 [(M+H)$^+$] (observed), 435.0529, 437.0508 [(M+H)$^+$] (calculated).

1,4-bis((6-bromohexyl)oxy)benzene (3a). Yield 65%; ^{1}H-NMR (400 MHz, $CDCl_3$): δ/ppm. 1.48-1.50 (m, -O(CH_2)$_2$(CH_2)$_2$(CH_2)$_2$Br, 8H), 1.75-1.78 (m, -O(CH_2)$_4$C$H_2$$CH_2$Br, 4H), 1.87-1.90 (m, -OCH_2CH_2(CH_2)$_4$Br, 4H), 3.42 (t, *J* = 6.8 Hz, -O(CH_2)$_4$$CH_2CH_2$Br, 4H), 3.91 (t, *J* = 6.4 Hz, -OC$H_2$$CH_2$($CH_2$)$_4$Br, 4H), 6.81 (s, -$H_{Ar}$, 4H). HRMS (m/z): 435.0559, 437.0533 [(M+H)$^+$] (observed), 435.0529, 437.0508 [(M+H)$^+$] (calculated).

Synthetic protocol of *N*,*N*,*N*′,*N*′-tetramethyl diaminohexyloxy benzenes (1b, 2b and 3b). $NHMe_2$ gas was collected into 20 mL chloroform solution of individual dibromohexyloxy benzene (**1a, 2a and 3a**) (1 g) in a sealed tube at 0 ˚C till the volume of the resulting solution was roughly doubled. Then, the reaction mixture was allowed to stir for 24 h at room temperature. Next, the reaction mixture was cooled and transferred into a RB. The solution was then kept in water bath to remove excess $NHMe_2$ followed by solvent evaporation by using rotary evaporator. Reaction mixture was then washed with 2 M aqueous KOH solution after dissolving it in $CHCl_3$. Finally, $CHCl_3$ layer was collected and evaporated to dryness to get a yellowish gummy liquid, **1b, 2b and 3b** with quantitative yield.

6,6'-(1,2-phenylenebis(oxy))bis(*N*,*N*-dimethylhexan-1-amine) (1b). ^{1}H-NMR (400 MHz, $CDCl_3$): δ/ppm. 1.36-1.40 (m, -O(CH_2)$_4$C$H_2$$CH_2$N($CH_3$)$_2$, 4H), 1.80-1.84 (m, -O($CH_2$)$_2$(C$H_2$)$_2$($CH_2$)$_2$N($CH_3$)$_2$, 8H), 1.79-1.83 (m, -O($CH_2$)$_4CH_2$$CH_2$N($CH_3$)$_2$, 4H), 2.20 (s, -$CH_2$N(C$H_3$)$_2$, 12H), 2.24-2.26 (m, -O(CH_2)$_2$$CH_2CH_2$N($CH_3$)$_2$, 4H), 3.99 (t, *J* = 6.6 Hz, -OC$H_2$$CH_2$($CH_2$)$_2$N($CH_3$)$_2$, 4H), 6.87 (s, -$H_{Ar}$, 4H). HRMS (m/z): 365.3154 [(M+H)$^+$] (observed), 365.3163 [(M+H)$^+$] (calculated).

6,6'-(1,3-phenylenebis(oxy))bis(*N*,*N*-dimethylhexan-1-amine) (2b). ^{1}H-NMR (400 MHz, $CDCl_3$): δ/ppm. 1.33-1.39 (m, -O(CH_2)$_4$C$H_2$$CH_2$N($CH_3$)$_2$, 4H), 1.44-1.84 (m, -O($CH_2$)$_2$(C$H_2$)$_2$($CH_2$)$_2$N($CH_3$)$_2$, 8H), 1.73-1.80 (m, -O($CH_2$)$_4CH_2$$CH_2$N($CH_3$)$_2$, 4H), 2.20 (s, -$CH_2$N(C$H_3$)$_2$, 12H), 2.24-2.26 (m, -O(CH_2)$_2$$CH_2CH_2$N($CH_3$)$_2$, 4H), 3.92 (t, *J* = 6.5 Hz, -OC$H_2$$CH_2$($CH_2$)$_2$N($CH_3$)$_2$, 4H), 6.44-6.48 (m, -$H_{Ar}$, 3H), 7.14 (t, *J* = 8.1 Hz, -H_{Ar}, 1H). HRMS (m/z): 365.3148 [(M+H)$^+$] (observed), 365.3163 [(M+H)$^+$] (calculated).

6,6'-(1,4-phenylenebis(oxy))bis(*N*,*N*-dimethylhexan-1-amine) (3b). ^{1}H-NMR (400 MHz, DMSO-d_6): δ/ppm. 1.23-1.31 (m, -O(CH_2)$_4$C$H_2$$CH_2$N($CH_3$)$_2$, 4H), 1.64-1.67 (m, -O($CH_2$)$_2$(C$H_2$)$_2$($CH_2$)$_2$N($CH_3$)$_2$, 8H), 1.64-1.67 (m, -O($CH_2$)$_4CH_2$$CH_2$N($CH_3$)$_2$, 4H), 2.08 (s, -$CH_2N^+$(C$H_3$)$_2$, 12H), 2.14-2.18 (m, -O(CH_2)$_2$$CH_2CH_2$N($CH_3$)$_2$, 4H), 3.89 (t, *J* = 6.5 Hz, -

OC*H*$_2$CH$_2$(CH$_2$)$_2$N(CH$_3$)$_2$, 4H), 6.81 (s, -*H*$_{Ar}$, 4H). HRMS (m/z): 365.3156 [(M+H)$^+$] (observed), 365.3163 [(M+H)$^+$] (calculated).

Synthetic protocol of ethyl ester bromide of phenylalanine (1c). Thionyl chloride (0.65 mL, 9 mmol) was added dropwise at 0-5 ˚C to 20 mL suspension of L-Phe (0.5 g, 3 mmol) in ethanol and the entire reaction mixture was refluxed for 12 h. Next, the excess ethanol and thionyl chloride were evaporated by rotary evaporator. The solid residue was washed with dry diethyl ether, resulted a white solid crude product. This crude white solid was dissolved in 10 mL of dichloromethane and potassium carbonate (1 g, 7.5 mmol) was added to the organic solution after dissolving it in 10 mL of distilled water. A solution of bromoacetyl bromide (0.4 mL, 4.5 mmol) in dichloromethane (10 mL) was then added dropwise to the reaction mixture at 5 °C for 1 h. The reaction mixture was stirred at room temperature for another 12 h. The aqueous solution was separated and the organic solution was washed with water and passed over the anhydrous Na_2SO_4 and concentrated to yield a white or yellowish white solid product with 80-94% yield.

Ethyl (2-bromoacetyl) phenylalaninate (1c). Yield 94%; ^{1}H-NMR (400 MHz, $CDCl_3$): δ/ppm. 1.24 (t, *J* = 7.1 Hz, -COOCH$_2$C*H*$_3$, 3H), 3.09-3.20 (m, -C*H*$_2$Ph, 2H), 3.85 (s, BrC*H*$_2$CONH-, 2H), 4.18 (q, *J* = 7.1 Hz, -COOC*H*$_2$CH$_3$, 2H), 4.79-4.83 (App quint., -*H*$_{(Phe)}$, 1H), 6.85-6.87 (br, -CON*H*, 1H), 7.12-7.28 (m, -*H*$_{Ar,}$ 5H). HRMS (m/z): 314.0336, 316.0396 [(M+H)$^+$] (observed), 314.0386, 316.0366 [(M+H)$^+$] (calculated).

General synthesis procedure of isoamphipathic antibacterial molecules (IAMs **1-3).** Individually, ethyl ester bromide intermediates, **1c** (2.8 equiv.) were reacted with *N, N, N′,N′*-tetramethyl diaminohexyloxy benzenes (**1b, 2b** and **3b**) (1 equiv.) in dry $CHCl_3$ (8-10 mL) at 65 ˚C. At the end of 24 h, reaction mixture was evaporated by using rotary-evaporator and the residue was dissolved in minimum amount of $CHCl_3$. The product was then precipitated by adding excess dry diethyl ether and the white residue was washed repeatedly with dry diethyl ether to remove the excess amount of activated ethyl ester bromides. The entire exercise resulted the generation of isoamphipathic antibacterial molecules (IAMs: **1-3**) with a quantitative yield. All the final molecules were characterized through ^{1}H-NMR, ^{13}C-NMR and HRMS.

IAM-1. ^{1}H-NMR (400 MHz, DMSO-d$_6$): δ/ppm.1.13 (t, *J* = 7.1 Hz, -COOCH$_2$C*H*$_3$, 6H), 1.26-1.31 (m, -O(CH$_2$)$_3$C*H*$_2$CH$_2$CH$_2$N$^+$(CH$_3$)$_2$-, 4H), 1.39-1.47 (m, -O(CH$_2$)$_2$C*H*$_2$(CH$_2$)$_2$CH$_2$N$^+$(CH$_3$)$_2$-, 4H), 1.63-1.75 (m, -OCH$_2$C*H*$_2$(CH$_2$)$_2$C*H*$_2$CH$_2$N$^+$(CH$_3$)$_2$-, 8H), 2.88-3.11 (m, -C*H*$_2$Ph, 4H and m, -CH$_2$CH$_2$N$^+$(C*H*$_3$)$_2$-, 12H), 3.35-3.39 (m, -CH$_2$C*H*$_2$N$^+$(CH$_3$)$_2$-, 4H), 3.94 (t, *J* = 6.6 Hz, -COOC*H*$_2$CH$_3$, 4H), 4.02-4.14 (m, -OC*H*$_2$(CH$_2$)$_5$N$^+$(CH$_3$)$_2$-, 4H), 4.02-4.14 (m, -NHCOC*H*$_2$N$^+$(CH$_3$)$_2$-, 4H), 4.52-4.60 (m, -*H*$_{(Phe)}$-, 2H), 6.85-6.96 (m, -*H*$_{Ar}$, 4H), 7.20-7.30 (m, -*H*$_{Ar\ (Phe),}$ 10H), 9.13 (d, *J* = 7.6 Hz -CON*H*, 1H). ^{13}C-NMR (100 MHz, DMSO-d$_6$): δ/ppm. 13.9, 21.7, 24.9, 25.3, 28.5, 51.2, 53.5, 60.9, 61.4, 61.5, 64.3, 68.1, 114.0, 120.9, 126.6, 128.2, 129.0, 136.6, 148.5, 163.2 and 170.6. HRMS (m/z): 416.2732 [(M-2Br)/2$^+$] (observed), 416.2670 [(M-2Br)/2 $^+$] (calculated).

IAM-2. ^{1}H-NMR (400 MHz, DMSO-d_6): δ/ppm. 1.13 (t, *J* = 7.1 Hz, -$COOCH_2CH_3$, 6H), 1.26-1.31 (m, -$O(CH_2)_3CH_2CH_2CH_2N^+(CH_3)_2$-, 4H), 1.40-1.43 (m, -$O(CH_2)_2CH_2(CH_2)_2CH_2N^+(CH_3)_2$-, 4H), 1.61-1.72 (m, -$OCH_2CH_2(CH_2)_2CH_2CH_2N^+(CH_3)_2$-, 8H), 2.90-3.17 (m, -$CH_2Ph$, 4H and m, -$CH_2CH_2N^+(CH_3)_2$-, 12H), 3.34-3.36 (m, -$CH_2CH_2N^+(CH_3)_2$-, 4H), 3.92 (t, *J* = 6.2 Hz, -$COOCH_2CH_3$, 4H), 4.02-4.12 (m, -$OCH_2(CH_2)_5N^+(CH_3)_2$-, 4H), 4.02-4.12 (m, -$NHCOCH_2N^+(CH_3)_2$-, 4H), 4.55-4.61 (m, -$H_{(Phe)}$, 2H), 6.43-6.50 (s, -H_{Ar}, 3H), 7.15 (t, *J* = 8.2 Hz, -H_{Ar}, 1H), 7.20-7.31 (m, -$H_{Ar\ (Phe),}$ 10H), 9.07 (d, *J* = 7.5 Hz, -CONH, 1H). ^{13}C-NMR (100 MHz, DMSO-d_6): δ/ppm. 13.8, 21.6, 24.5, 25.3, 28.3, 51.3, 53.5, 61.0, 61.4, 67.1, 114.2, 120.8, 126.7, 128.3, 129.0, 136.5, 148.4, 159.8, 163.1 and 170.6. HRMS (m/z): 416.2737 [(M-2Br)/2$^+$] (observed), 416.2670 [(M-2Br)/2$^+$] (calculated).

IAM-3. ^{1}H-NMR (400 MHz, DMSO-d_6): δ/ppm. 1.13 (t, *J* = 7.1 Hz, -$COOCH_2CH_3$, 6H), 1.25-1.29 (m, -$O(CH_2)_3CH_2CH_2CH_2N^+(CH_3)_2$-, 4H), 1.39-1.44 (m, -$O(CH_2)_2CH_2(CH_2)_2CH_2N^+(CH_3)_2$-, 4H), 1.63-1.71 (m, -$OCH_2CH_2(CH_2)_2CH_2CH_2N^+(CH_3)_2$-, 8H), 2.90-3.35 (m, -$CH_2Ph$, 4H and m, -$CH_2CH_2N^+(CH_3)_2$-, 12H), 3.88 (t, *J* = 6.4 Hz, -$COOCH_2CH_3$, 4H), 3.98-4.10 (m, -$OCH_2(CH_2)_5N^+(CH_3)_2$-, 4H), 3.98-4.10 (m, -$NHCOCH_2N^+(CH_3)_2$-, 4H), 4.55-4.60 (m, -$H_{(Phe)}$, 2H), 6.82 (s, -H_{Ar}, 4H), 7.22-7.31 (m, -$H_{Ar\ (Phe)}$, 10H), 9.08 (d, *J* = 7.7 Hz, -CONH, 2H). ^{13}C-NMR (100 MHz, DMSO-d_6): δ/ppm. 13.9, 21.7, 25.0, 25.4, 28.4, 51.2, 53.5, 60.9, 61.3, 64.3, 67.6, 115.2, 126.6, 128.2, 129.0, 136.6, 152.6, 163.2 and170.6. HRMS (m/z): 416.2660 [(M-2Br)/2$^+$] (observed), 416.2670 [(M-2Br)/2$^+$] (calculated).

Antibacterial assay. [1,2]At first bacteria from the frozen stock (at -80 ˚C) were streaked either on nutrient broth (for Gram-positive bacteria) or MacConkey agar plate (for Gram-negative bacteria). The streaked plates were then incubated overnight at 37 ˚C for bacterial growth. A single bacterial colony was next inoculated for 6 h (midlog phase) in 3 mL of nutrient broth to produce about 10^8 to 10^9 CFU/mL cells depending upon the nature of the bacteria. The 6 h grown culture was diluted to ~10^5 CFU/mL which was then used for antibacterial assay determination. Compounds were 2-fold serially diluted in a 96-well plate from the starting concentration using sterile Millipore water. Afterward, 180 µL of ~10^5 CFU/mL bacterial solution was added in each well containing 20 µL aqueous solution of the test compound. The plates were then incubated for 16-18 h at 37 ˚C in shaking condition. The O.D at 600 nm was recorded by using TECAN (Infinite series, M200 PRO) plate reader. Each concentration was triplicate and the experiment was performed twice and the antibacterial activity (MIC) was evaluated based on visual turbidity.

Antibacterial activity upon human blood plasma and serum pre-incubation. [2] Human blood was centrifuged at 3500 rpm for 5 min and the plasma was collected carefully from the supernatant. Similarly, human blood was collected into BD Vacutainer® Serum Tubes and further centrifuged at 3500 rpm to obtain human blood serum. Next, 500 µL of 512 µg/mL (515.6 µM) solution of IAM-**1** in 1×PBS was mixed with equal volume of blood plasma/serum and the individual mixtures were incubated for different time points (1 h, 2 h, and 3 h) at 37 ˚C. At the end of specific incubation time, each mixture was subjected for 2 fold serial

dilutions and MIC was conducted with them by following the aforementioned protocol against MRSA.

Hemolytic activity.[2,3] Aqueous solution of individual compounds (IAMs: **1-3**) were serially diluted by two fold in triplicate in a 96-well plate. Freshly collected human blood (heparinized) was then centrifuged down and supernatant was thrown away to collect the human red blood cells (hRBCs). Later, collected hRBCs (5 vol %) were slowly suspended using 1×PBS (pH = 7.4). Next, 150µL of this suspension was added to the wells of 96 well plates containing 50 µL compound's solution and plate was allowed to incubate at 37 ˚C for 1 h. Then centrifugation at 3500 rpm for 5 min was performed and the supernatant (100 µL) was then transferred to another 96-well plate for recording the absorbance at 540 nm by using Tecan Infinite M200 PRO microplate reader. In this study, same volume of 1×PBS without compound served as a negative control whereas same volume of Triton X-100 (1 vol% solution in 1×PBS) was used as a positive control. The percentage of hemolysis was determined by using the following formula: $(A_{treat} - A_{nontret}) / (A_{TX\text{-}treat} - A_{nontret}) \times 100$, where A_{treat} corresponds to the absorbance of the compound-treated well, $A_{nontret}$ stands for the absorbance of the negative controls (without compound), and $A_{TX\text{-}treat}$isthe absorbance of the triton-X-100 treated well. Each concentration had triplicate values and the HC_{50} was determined by considering the average of triplicate O.D.

Co-culture study

Co-culture with MRSA and human erythrocytes.[4] MRSA and human erythrocytes were mixed with each other in 1×PBS in such way so that their effective concentration remained as ~10^7 CFU/mL and ~10^8 hRBCs/mL. Next, 180 µL of the co-culture suspension was treated individually with 20 µL of IAM **1-3** at 2560 µg/mL (2578 µM) [working concentration: 256 µg/mL (257.8 µM)]. After 15 min incubation at 37 ˚C in a stationary condition, 20 µL of the suspension was withdrawn and 10-fold serially diluted followed by spot plating each dilutions on nutrient agar plates for counting viable MRSA cells. Finally, at the end of 24 h incubation, the viable bacterial colonies were counted and the results were expressed in percentage with respect to the untreated MRSA count in co-culture condition. On the other hand, the reaming volume of MRSA and hRBC suspension was centrifuged at 3500 rpm for 5 min and the absorbance of the supernatant (100 µL) was recorded at 540 nm by using Tecan Infinite M200 PRO microplate reader. In this study, same volume (20 µL) of triton-X (1 vol% solution in 1×PBS) instead of test compound was used as a positive control for determination of hRBC lysis. The percentage of hemolysis was determined by using the following formula: $(A_{tret} - A_{nontret}) / (A_{TX\text{-}tret} - A_{nontret}) \times 100$, where A_{tret} corresponds to the absorbance of hRBCs in co-culture condition upon compound treatment , $A_{nontret}$ stands for the absorbance of hRBCs in co-culture condition without compound treatment, and $A_{TX\text{-}tret}$ is the absorbance of hRBCs in co-culture condition upon triton-X treatment.

Co-culture with MRSA and RAW cells.[5]RAW 264.7 cells (~10^5 cells/well) were seeded onto the wells of a 96-well plate in DMEM media (supplemented with 10% FBS and 5% penicillin-

streptomycin) at 37 ˚C with 5 % CO_2 atmosphere for 12 h. Afterward, cell culture medium was discarded and cells were treated with 100 µL of freshly prepared MRSA (~ 10^5 CFU/mL) supplemented with 256 µg/mL (257.8 µM) compound solution (IAM-**1** or IAM-**2** or IAM-**3**) in antibiotic free DMEM media with 10% FBS. Two controls were included in the study, in one case the MRSA cells were left untreated with compound in presence of RAW cells and in other case, RAW cells were left untreated with both compound as well as MRSA where same volume of antibiotic-free DMEM (supplemented with 10% FBS) was added. The plate was then incubated for 3 h at 37 ^oC under 5% CO_2 atmosphere. To determine the bacterial cell viability, 20 µL of the suspension was withdrawn and 10-fold serially diluted followed by spot plating each dilution on nutrient agar plates for counting viable MRSA cells. Finally, at the end of 24 h incubation, the viable bacterial colonies were counted and the results were expressed in percentage with respect to the untreated MRSA count in co-culture condition. On the other side, RAW cells viability was also determined by performing Alamar blue assay (chapter 2, section 2.4.12) with the reaming supernatant and results were represented in terms of percentage by considering 100% cell viability in case of RAW cells devoid of MRSA and compound treatment.

Membrane fluidity study.[6,7] 0.5 mM of DPPG : DPPE (88 : 12) and 0.5 mM of DPPC lipids along with laurdan dye (5 mM) were dissolved in minimal volume of analytical grade chloroform in a 10 mL RB. Next, a thin layer films with the lipids were made within the walls of RB by applying argon flow. Further, the thin films were dried under vacuum for 1 h. Then, 10 mL of 1×PBS (pH = 7.4) was added on the lipid films and incubated for 12 h at 4-8 ˚C for hydration. Further, 10 freeze-thaw cycles (from 70 ˚C to 4 ˚C with intermittent vortexing) were executed with the hydrated films. These multilamellar vesicles were finally sonicated at 70 ˚C for 15 min to obtain unilamellar vesicles. The freshly prepared liposome solution (2 mL) was taken into 3 mL fluorescence cuvette and the emission intensity was measured at 440 nm upon excitation at 350 nm. Similarly, the emission intensity was measured upon IAMs **1-3** treatment at 256 µg/mL (257.8 µM) in case of both bacterial and mammalian membrane mimicking liposomes.

Membrane leakage study.[6,7] To investigate dye leakage upon IAM **1-3** treatment through fluorescence spectroscopy, vesicles entrapped with 30 mM 5(6)-Carboxyfluorescein (CF) dye was prepared in 1×PBS buffer (pH = 7.4). In high concentrations (30 mM), CF does not emit due to self-quenching and displays significant emission at diluted condition of 3 mM concentration. Bacterial membrane mimicking vesicles were prepared using 0.5 mM DPPG and DPPE lipid (88 : 12) in CF solution (30 mM) in 1×PBS buffer by following the previously mentioned protocol. Mammalian membrane mimicking vesicles were also prepared in the similar way using 0.5 mM DPPC lipid. However, herein, each freeze-thaw cycle was accompanied with sonication for 30 s. Further, vesicle untapped dye was removed from the solution using size exclusion chromatography. Sephadex G-50 was used as the stationary phase and 1×PBS was used as the eluent. Finally, 200 µL of vesicles were equilibrated with 1.8 mL 1×PBS and emission intensity was recorded at 517 nm using an

excitation at 495 nm. In control case, instead of test compound solution, water was added at 50 s and fluorescence intensity was measured upto 200 s. Likewise, fluorescence intensity was recorded upon treating bacterial and mammalian membrane mimicking vesicles individually with IAM **1-3** [160 μg/mL (161 μM)] at 50 s followed by addition of 1% triton-X at 200 s. The fluorescence intensity obtained after triton-X treatment in case of control was used for normalization. Further, rate constant of dye leakage was calculated by fitting each emission spectrum from t = 50 s (after addition of IAM) to t = 200 s (before addition of triton-X) using exponential rise equation ($y = y_0 + A_1e^{-x/t_1}$). The rate constant was considered ask = $1/t_1$.

Water-membrane partition experiments

Liposomes were prepared by extrusion, as previously described, with lipid compositions: POPE/POPG (7:3, mol/mol) and POPC/Cholesterol (1:1, mol/mol), as mimics of bacterial and eukaryotic membranes, respectively. The lipid film was hydrated with a 10 mM phosphate buffer (pH=7.4), prepared by using ultrapure water and containing 140 mM NaCl and 0.1 mM EDTA (buffer A henceforth). Liposomes were separated from unencapsulated dye by gel filtration on a 40 cm Sephadex G-50 column. The final lipid concentration was determined according to the Stewart phospholipid assay.[8]

A fixed IAM concentration (10 μM) was titrated with increasing concentrations of liposomes. After each addition, the fluorescence spectra were recorded repeatedly until no further changes were observed (about 5-10 minutes). Control experiments to check for possible effects of sample turbidity on the fluorescence signal were performed by repeating the same titration with tryptophan.

The fraction of IAM associated to membranes (f_b) was calculated from the fluorescence intensity (F, at the wavelength of 318 nm), according to the following equation:

$$f_b = \frac{(F - F_w)}{(F_b - F_w)} \tag{1}$$

where F_b and F_w refer to the fluorescence signal of bound and free IAM, respectively. F_b was determined by extrapolating the titration with the following equation:

$$F = F_W + (F_b - F_W)\frac{K_p \cdot \frac{[L]}{[W]}}{1 + K_p \cdot \frac{[L]}{[W]}} \tag{2}$$

where K_p represents the lipid/water partition constant, $[L]$ is the molar concentration of lipids in the sample and $[W]$ is the molar concentration of pure water at 25 °C (55.5 M). In Equation 2, the lipid concentration dependence of the fraction of bound IAM was described by the following equation, corresponding to an ideal partition equilibrium model.[8,9]

$$f_b = \frac{K_p \cdot \frac{[L]}{[W]}}{1 + K_p \cdot \frac{[L]}{[W]}} \quad (3)$$

The partition curves of the POPC/Cholesterol neutral liposomes were too far from the plateau to allow extrapolation. Therefore, the value of the bound state fluorescence F_b determined for the POPE/POPG liposomes was used for the POPC/Cholesterol vesicles, too, assuming that the membrane composition does not affect significantly the fluorescence in the bound state. In principle, the turbidity of the liposome solution might artifactually cause variations in the fluorescence signal. However, negative control experiments with tyrosine (which does not bind to vesicles) showed no significant changes in the emission spectra, demonstrating the absence of any relevant scattering-related artefacts.

Molecular dynamics simulations

The force field parameters for IAM compounds were obtained by starting from the ATB server.[10] The charges were slightly modified to preserve the symmetry of the molecules and in analogy with those of analogous groups in the GROMOS 54A7 force field.[11] The hydrophobic chains in the compounds were modeled with the Berger parameters used for lipids (see below).

In simulations of the IAM molecules in water, a single copy of the compound was placed at the center of a box (44 nm^3) and hydrated with approximately 1400 pre-equilibrated simple point charge (SPC) water molecules. 6 Cl^- and 4 Na^+ ions were added to ensure electroneutrality and a ionic strength roughly corresponding to 0.150 M. MD simulations were carried out with the GROMACS 2020.6 software package.[12] Each system was energy-minimized and then equilibrated during a 100 ps MD, where the positions of the IAM atoms were restrained. Production simulations were performed at least in triplicate, for a total amount of almost 12 μs of simulation time at a temperature of 300 K, with the same parameters and settings used in the membrane simulations (see below).

The most representative structures of each simulation were defined by cluster analysis conducted with GROMACS (cluster tool), using a 0.25 nm root mean square deviation cutoff.

MD simulations of IAM-1 in presence of membrane lipids were performed with the "minimum bias" approach, which minimizes the effect of the initial configuration on the final results. In this method, the simulation is started from a random mixture of the membrane-active molecule, lipids and water, and the bilayer forms spontaneously, usually in 50–100 ns. During this self-assembly process, the system is very fluid, particularly in the first stages of the simulation, thus ensuring that the bioactive molecule can sample different environments in a relatively short time, and, as a consequence, it can find its minimum free energy configuration. We demonstrated that the simulative results obtained with this approach are consistent with the depth of membrane insertion and the orientation

determined experimentally by fluorescence, ATR-FTIR and solid-state NMR spectroscopies.[13-15] Membranes of POPE/POPG (90:38) were used to parallel the conditions of the experimental studies on lipid vesicles and to mimic bacterial membranes. Briefly, a single copy of the compound was placed at the center of a 9 × 9 × 9 nm box. 128 lipid molecules and 7500 water molecules were randomly added into the box. 38 Na^+ atoms were introduced in replacement of water molecules, as counterions of the negative charges on the lipids, and 2 Cl^- atoms as counterions of the +2 charge on the compounds. MD simulations were carried out with the GROMACS 2020.6 software package. The parameters for the lipids were taken from the literature.[16] Temperature was controlled using a velocity-rescaling thermostat.[17] Pressure coupling was applied using the Parrinello-Rahman barostat, with a time constant of 1.0 ps and a reference pressure of 1 bar.[18] All bond lengths were constrained with the LINCS algorithm.[19] Short-range electrostatic interactions were cut-off at 1.4 nm and long-range electrostatic interactions were calculated using the particle mesh Ewald (PME) algorithm.[20] Simulations were run with a 2 fs time step. Each system was energy minimized and then equilibrated using a 100 ps MD, where the positions of the IAM atoms were restrained. At first, simulations were performed for 200 ns, at a temperature of 310 K, with anisotropic pressure coupling. In cases where this time was not sufficient to attain a defect-free bilayer, the system was annealed by cycling the temperature between 310 K and 375 K, for further 120 ns, followed by a production run with semi-isotropic pressure coupling. Analyses were conducted on the last 20 ns of the simulations. The density profiles along the bilayer normal were determined by means of the "gmx density" tool in GROMACS.

Molecular graphics images were produced using the UCSF Chimera package from the Resource for Biocomputing, Visualization, and Informatics at the University of California, San Francisco (supported by NIH P41 RR-01081).[21]

Membrane active mechanism of action. [1-3]

Cytoplasmic Membrane Depolarization Assay. Midlog phase (working concentration: ~10^8 CFU/mL) MRSA cells were collected separately (centrifugation at 3500 rpm for 5 min), and washed with 1:1 ratio of 5 mM glucose and HEPES buffer (pH = 7.4). Next, the bacterial plate was resuspended in 1:1:1 ratio of 5 mM HEPES buffer, 100 mM KCl solution supplemented with 0.2 mM EDTA and 5 mM glucose. For this study EDTA was used to allow the dye uptake by permeabilizing outer membrane of *A. baumannii*. This study was performed in a Corning 96 black well plate with clear bottom containing 2 µM of 3,3'-dipropylthiadicarbocyanine iodide [$DiSC_3(5)$] and 190 µL of bacterial suspension. After 60 min incubation of the plate, fluorescence intensity was measured at 622 nm excitation wavelength and 670 nm emission wavelength for 4 min. After that, 10 µL of IAM-**1** (at working concentration of 16 µg/mL and 32 µg/mL) was mixed with the suspension of bacteria and dye of each well. Same volume of water without compound was used as the control for this experiment. Increment in

fluorescence intensity was measured for another 25 min using Tecan Infinite M200 PRO microplate reader.

Outer Membrane (OM) Permeabilization Assay. Midlog phase *E. coli* cells were independently harvested, washed with 1:1 mixture of 5 mM HEPES buffer and glucose and resuspended with the same. The working concentration of midlog phase and stationary phase bacteria were ~10^8 CFU/mL. This study was performed in a Corning 96-black well plate with clear bottom containing 10 µM of *N*-Phenyl naphthylamine (NPN) dye and 190 µL of bacterial suspension. Then, the fluorescence was monitored for first 4 min at excitation wavelength of 350 nm and emission wavelength of 420 nm. After that, bacterial suspension with dye at each well was treated with 10 µL of test compound, IAM-**1** at working concentrations of 16 µg/mL and 32 µg/mL. The same volume of water without a compound was used as the control for this experiment. An increase in fluorescence intensity was monitored for another 25 min with Tecan Infinite M200 PRO microplate reader.

Bacterial live/dead assay.[1]IAM-**1** [16 µg/mL (16 µM)] was added to 1 mL of ~10^8 CFU/mL midlog phase MRSA suspension in normal saline and was incubated at 37 ˚C. After 6 h of incubation, bacterial suspension was centrifuged to remove the compound completely. Then, the bacterial palate was resuspended with normal saline followed by the addition of 5 µL of Syto-9 (3 µM) and PI (15 µM) mixture and incubated for half an hour. Further, the dye containing bacterial suspension was centrifuged to remove the excess unbound dye and the palate was resuspended with 50 µL of normal saline. Finally, 5 µL of bacterial suspension was taken into a glass slide and processed for confocal microscopy at 63 X resolution.

Cytotoxicity assay.[2]

Alamar blue Assay. Cytotoxicity of IAMs: **1-3** was examined against Raw 264.7 cell line by Alamar blue assay. Briefly, cells (~10^4 cells/well) were seeded onto the wells of a 96-well plate in DMEM media supplemented with 10% fetal bovine serum (FBS) and 5% penicillin-streptomycin. Then 100 µL of serially diluted compound solution in DMEM media was added to the each well of the plates containing the cells. The same volume of media (untreated cells) and the cells treated with 0.1% (v/v) Triton-X solution was taken as positive and negative control respectively. The plates were then kept for incubation at 37 ˚C for 24 h maintaining 5% CO_2 atmosphere. Afterward, 10 µL of 10 x Alamarblue solution was added to each well followed by 4 h of further incubation at the same condition. Then, the absorbance was recorded at 570 nm wavelength and 600 nm wavelength was used as the reference. The percentage of cell viability was calculated using the following equation: cell viability (%) = $(A_c - A_t)/(A_0 - A_t) \times 100$, where A_c indicates the absorbance for cells treated with compound, A_t is the absorbance for the cells treated with 0.1% (v/v) Triton-X and A_0 is the absorbance of the untreated cells, all at 570 nm. Each concentration had triplicate values, and the average of triplicate absorbance values was plotted against concentration followed by fitting with a sigmoidal plot.

Fluorescence Microscopy. ~10^4 cells (HEK 293) were seeded into the individual wells of a 96-well plate. Then 100 µL of 256 µg/mL of IAMs: **1-3** was added over the seeded cells. 0.1% Triton-X treated and untreated cells were considered as positive and negative controls respectively. After single time washing with 1×PBS the untreated and treated cells were then stained with 50 µL of 1:1 calcein-AM (2 µM) and propidium iodide (PI) (4.5 µM) for 15 min under 5% CO_2 atmosphere at 37 ˚C. Finally, the excess dyes were removed by washing the cells with 1×PBS, and images were captured at 40×objective with the help of a Leica DM2500 fluorescence microscope. During imaging, a band-pass filter for calcein-AM (at 500−550 nm) and a long-pass filter for PI (at 590−800 nm) were used.

Bactericidal kinetics.[2] A single colony of MRSA and *E. coli* was inoculated separately in nutrient broth for 6 h at 37 ˚C to produce 10^8 CFU/mL to 10^9 CFU/mL cells. Next, this midlog phase bacterial solution was further diluted to ~5× 10^5 CFU/mL and 180 µL of this diluted bacterial solution in Mueller Hinton broth was added to the 20 µL aqueous solution of test compound**,** IAM-**1** with the concentration of 16 µg/mL (16.1 µM), 32 µg/mL (32.2 µM) for MRSA and 32 µg/mL (32.2 µM) and 64 µg/mL (64.4 µM) for *E. coli*. The same volume of autoclaved water without the test compound was used as a control. Afterward, 20 µL of aliquots from the individual mixture of bacteria and compound were serially diluted by 10-fold in sterile saline at different time points (0 h, 1 h, 2 h, 4 h, 6 h, and 12 h). Then, spot plating on agar plates was executed with 20 µL solution from each dilution and allowed to incubate for 24 h at 37 ˚C. Finally, the number of bacterial colonies was counted and results were presented in logarithmic scale, i.e., Log (CFU/mL) vs time.

Activity against stationary and persister cells.[2,3]A midlog phase (6 h grown culture) MRSA and *E. coli* culture was diluted to 1:1000 ratio in nutrient broth and incubated at 37 ˚C for 16 h in shaking condition to achieve stationary phase cells. Later on, the bacterial suspension was centrifuged (9000 rpm, 2 min) and resuspended in 1xPBS. On the other hand, the persister cells were generated from the stationary phase cells upon specific antibiotic exposure for 3 h. 1 mL of stationary phase culture was treated with 100 µg/mL (for *S. aureus*) and 300 µg/mL (for *E. coli*) of ampicillin sodium for 3 h at 37 ˚C. Next, the bacteria were centrifuged, washed 3-4 times, and resuspended in 1xPBS to remove the traces of the antibiotic. Finally, 180 µL of the stationary and persister phase bacteria (~5× 10^5 CFU/mL) was added to 20 µL of IAM-**1** solution with the concentrations of 16 µg/mL (16.1 µM), 32 µg/mL (32.2 µM) for stationary phase MRSA and persister phase *S. aureus* and 32 µg/mL (32.2 µM), 64 µg/mL (64.4 µM) for both stationary and persister phase *E. coli*. Similarly, for vancomycin (stationary phase MRSA and persister phase *S. aureus*) and colistin (for both stationary and persister phase *E. coli*) antibiotic concentrations were 64 µg/mL (64.4 µM) and 32 µg/mL (27.7 µM) and same volume of water without compound was considered as an untreated control. After 6 h time, 20 µL aliquots from that solution were serially diluted 10-fold in sterile saline. Then 20 µL solution from each dilution was spot plated on MacConkey agar plates and after 24 h of incubation at 37 ˚C, the number of bacterial colonies was

counted. The results were presented in a bar plot in logarithmic scale, i.e. Log (CFU/mL) at 6 h time point.

Biofilm disruption assay. [2,3]

Crystal Violet Staining. Biofilm disruption study was conducted over coverslips of diameter 13 mm. First, 6 h grown culture of MRSA ATCC33591 (midlog phase) was diluted to 10^5 CFU/mL in nutrient broth, supplemented with 1% glucose and 1% NaCl. Then this diluted bacterial suspension (2 mL/well) was added to wells containing the sterilized coverslips and the plate was allowed to incubate at static condition at 37 ˚C for 24 h. Then, after removal of media, biofilm containing coverslips were cautiously washed with 1×PBS (pH = 7.4) to remove the planktonic bacteria and coverslips were then placed into the well of a new 6-well plate. Afterward, two solutions (2 mL) of IAM-**1** with two different concentrations [64 μg/mL (64.4 μM) and 128 μg/mL (128.9 μM)] were added to the wells containing biofilm coated coverslip incubated for 24 h. As an untreated control, 2 mL of fresh media without compound was added to the well. For this study, vancomycin at 64 μg/mL (44.2 μM) was used as the antibiotic control. After 24 h, 1×PBS was used to wash the planktonic cells from the coverslips. Later on, all the compound treated and untreated coverslips were carefully positioned into another 6-well plate. To visualize biofilm disruption, those coverslips were incubated with 1 mL of 0.1% of crystal violet (CV) dye in the 6-well plate and allowed to incubate for 10 min. After washing with 1× PBS, the crystal violet associated with the biofilm containing coverslip was dissolved in 95% ethanol and absorbance was recorded at 520 nm. The amount of biomass left on the coverslips was indicated by the absorbance of CV dye.

Cell Viability of Biofilm Embedded Bacteria. In this case, an aforementioned protocol was followed for biofilm growth and treatment with IAM-**1** and antibiotics. After placing the washed coverslips containing biofilm into a fresh well plate, 2 mL of trypsin-EDTA solution diluted in saline (1:4 ratios) was added and allowed to incubate for 10-15 min with shaking. 20 μL of the bacterial suspension was then 10-fold serially diluted and each dilution was spot plated on nutrient agar plates. The spotted plates were then incubated for 24 h. At the end of incubation, the viable bacterial colonies were counted and the results were expressed as Log (CFU/mL).

Cell Viability of Biofilm Disseminated Bacteria. To quantify the viability of biofilm disseminated bacterial cells, 20 μL of dispersed cell suspension present in the biofilm growing media was serially 10 fold diluted in 0.9% saline and 20 μL of the diluted solutions was spot plated on nutrient agar plate and allowed to incubate for 18 h at 37 ˚C. Afterward, the viable bacterial colonies were counted.

Confocal Laser-Scanning Microscope (CLSM) of Biofilms. Like the previous studies, the optimized molecule, IAM-**1** had been used for this experiment. The treated and untreated coverslips (previously described in biofilm disruption assay section) were placed on glass slides after washing with 1×PBS. The biofilms staining was performed with 5 μL of Syto-9 (60

μM) and PI (15 μM) dye mixture and images were captured with the help of a Zeiss 510 Meta confocal laser-scanning microscope. Image J was used to process the images. Further, the percentage of live and dead cell ratio was calculated through Image J using the following formula.

% live cells = [(No of cells stained with green colour-No of cells stained with red colour) x100]/No of cells stained with green colour

% Dead cells = (100 - % of live cells)

Dermal Toxicity.[2] The study was executed by following OECD guidelines (OECD 425). Briefly, three groups of mice (n = 4) were used for this experiment. First, the mice were anesthetized by using 150 μL of xylazine-ketamine cocktail through intraperitoneal injection. Then, fur from the dorsal area (~1/10th of total body surface) of mice were removed carefully without any skin injury. Afterward, IAM-**1** with 200 mg/kg dosage in saline was applied to the shaved portion of one group of mice. Other group of mice was also treated with saline without any compound. The compound treated group of mice was continuously monitored for first 2 h from the initial experimental time point. Later on, both group of mice was monitored for another 14 days. On 7^{th} day of post treatment, one group of mice treated with IAM-1 were sacrificed through cervical dislocation and the dermal tissues were isolated in 10% neutral buffer formalin (NBF) in order to analyse histopathological changes through hematoxylin and eosin staining. Similarly, other group of mice treated with IAM-**1** were also sacrificed on 14^{th} day and their dermal tissues were subjected to histopathological analysis. This part of the experiment was performed at Rohana Veterinary Diagnostic laboratory (Bangalore, Karnataka, India).

***In-vivo* antibacterial assay.** 6-8 week BALB/C CD-1 female mice with average body weight of 22 g were assigned as 4 number in each treatment group. First, the mice were anesthetized by using 150 μL of xylazine-ketamine cocktail through intraperitoneal injection. Then, fur from the dorsal area (~1/10th of total body surface) of mice was removed carefully without any skin injury. Next, a wound was created on the dorsal area using scalpel. Then, the wound site was infected with 20 μL of 10^7 CFU midlog phase (6 h grown) MRSA ATCC 33591 in 1×PBS. The treatment with IAM-**1** (40 μL in 1×PBs, 80 mg/kg, once in a day) and vancomycin (40 μL in 1×PBS, 50 mg/kg, once in a day) was started after 4 h post infection upon topical application. The treatment was continued for next 5 consecutive days. In case of control group of mice, 40 μL of 1×PBS was applied topically for total 5 days. Finally, at 6^{th} day, all the group of mice were euthanized through cervical dislocation and the infected skin tissue were collected aseptically in 10 mL saline. In general, the weight of the mice dermal tissue was in the range of 0.16-0.46 g. Next, these tissues were homogenised in 10 mL saline and the number of MRSA in this infected tissue was tittered. The bacterial count was expressed in Log CFU/gm.

Supplementary Figures

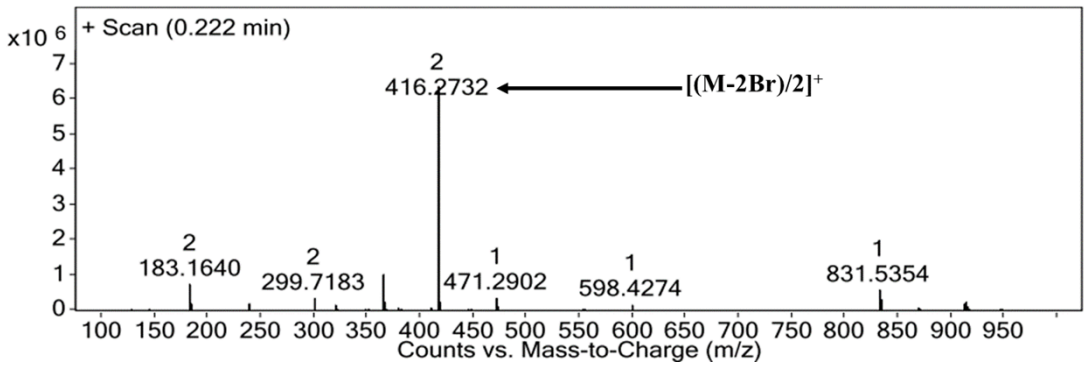

Figure S1. HRMS of **IAM-1**.

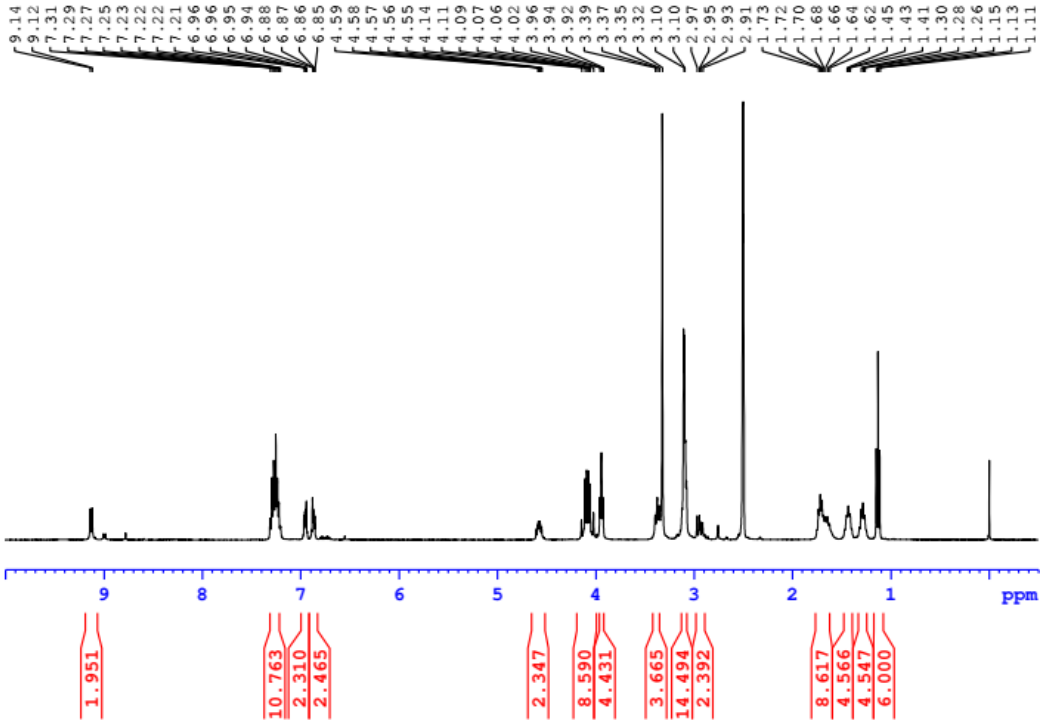

Figure S2. ^{1}H-NMR of IAM-**1**. The NMR was taken in DMSO-d6 and the solvent peak was calibrated at the δ value of 2.5 ppm.

.

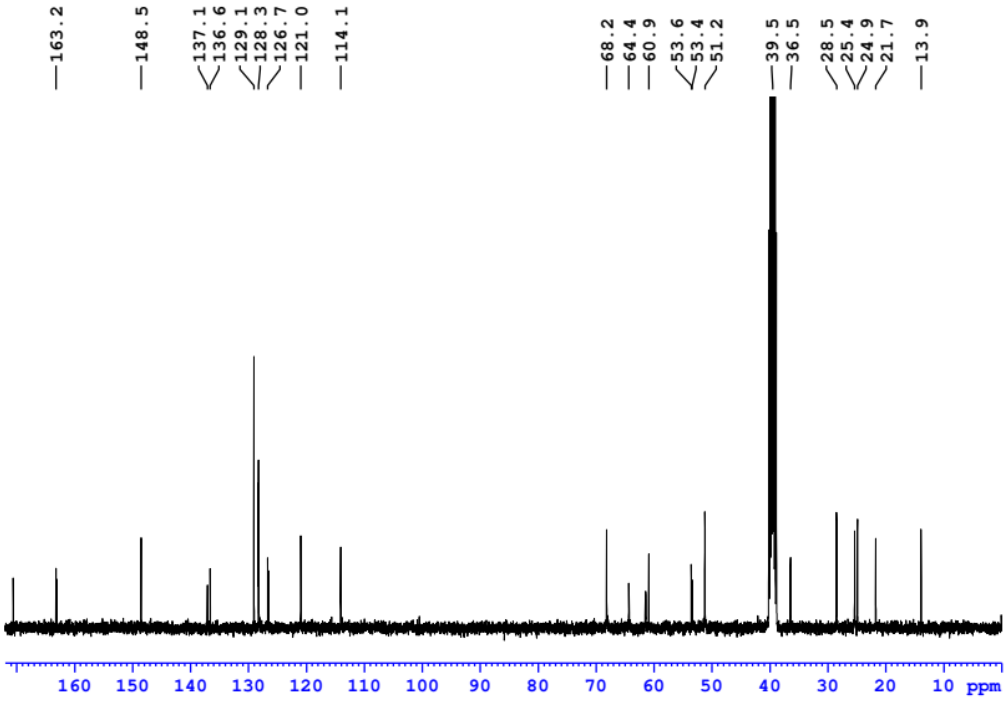

Figure S3. ^{13}C-NMR of **IAM-1**. The NMR was taken in DMSO-d_6 and the solvent peak was calibrated at the δ value of 39.52 ppm.

.

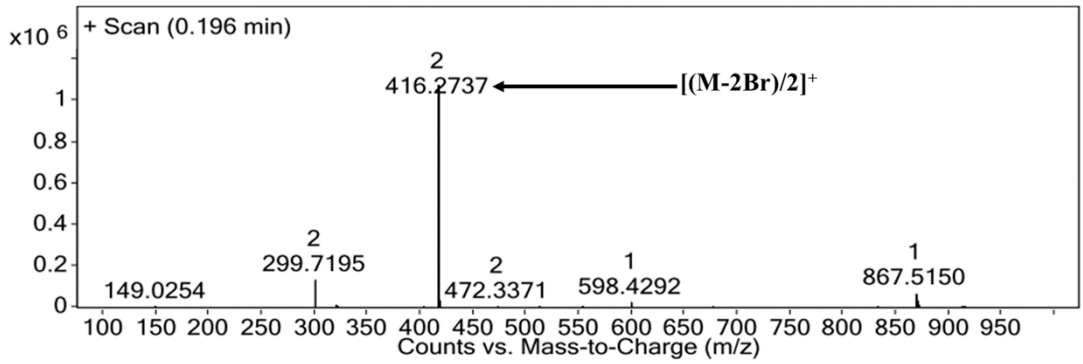

Figure S4. HRMS of **IAM-2**.

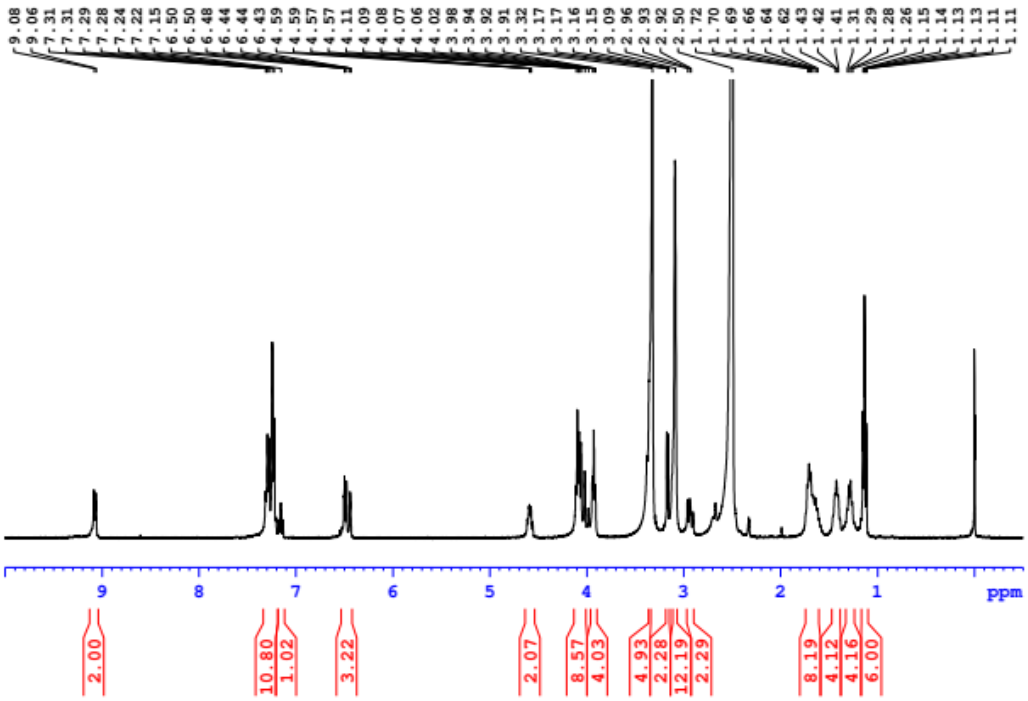

Figure S5. [1]H-NMR of IAM-**2**. The NMR was taken in DMSO-d6 and the solvent peak was calibrated at the δ value of 2.5 ppm.

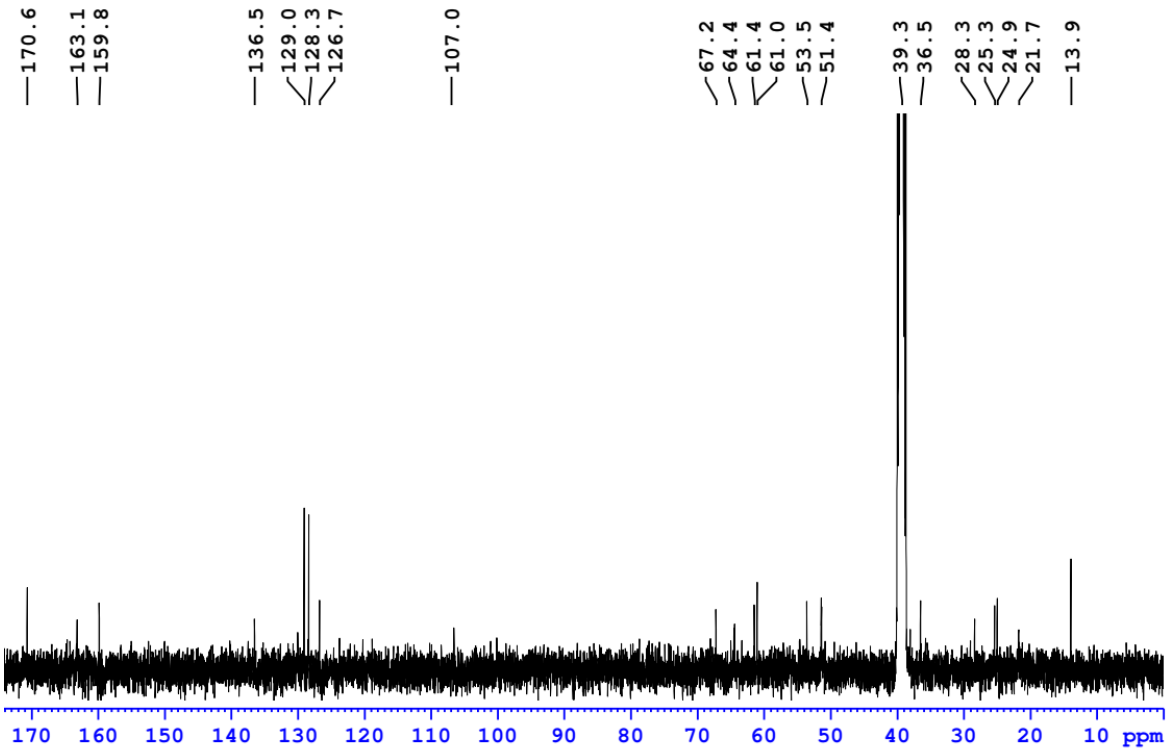

Figure S6. [13]C-NMR of **IAM-2**. The NMR was taken in DMSO-d_6 and the solvent peak was calibrated at the δ value of 39.52 ppm.

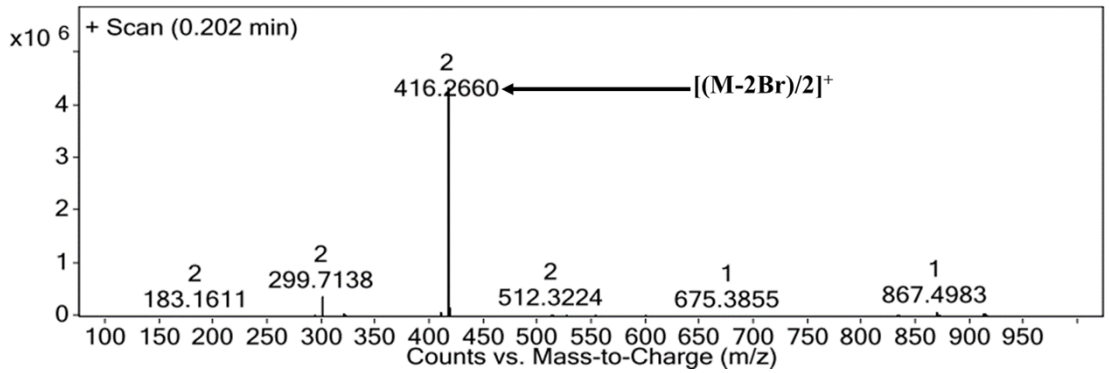

Figure S7. HRMS of **IAM-3**.

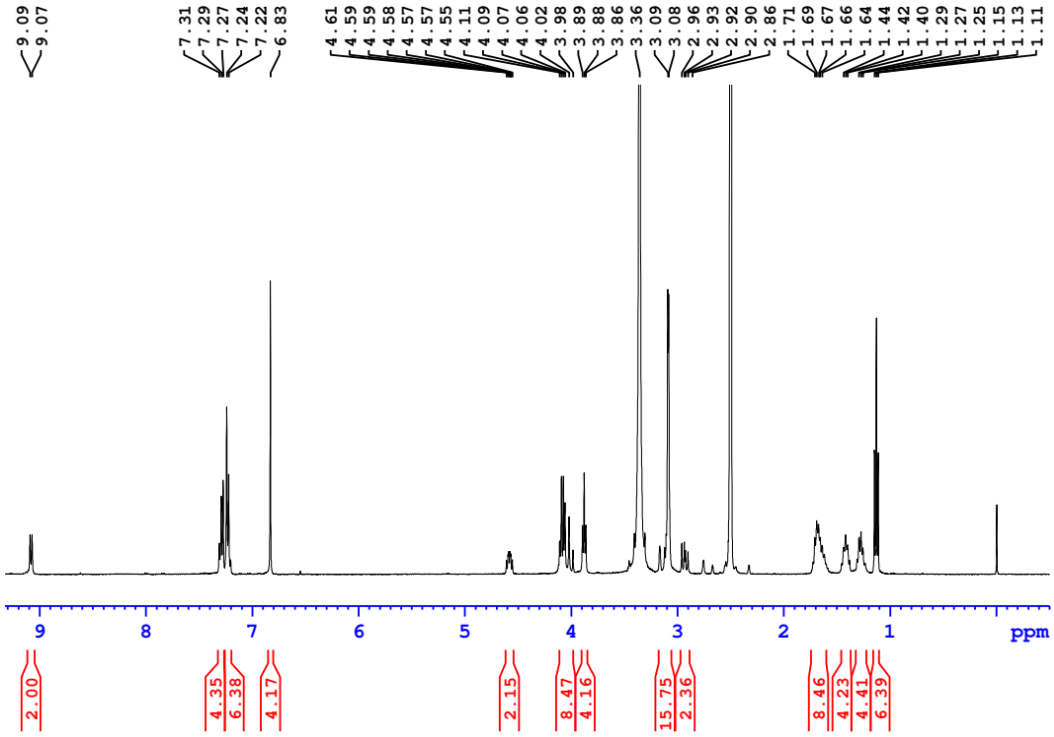

Figure S8. [1]H-NMR of IAM-**3**. The NMR was taken in DMSO-d6 and the solvent peak was calibrated at the δ value of 2.5 ppm.

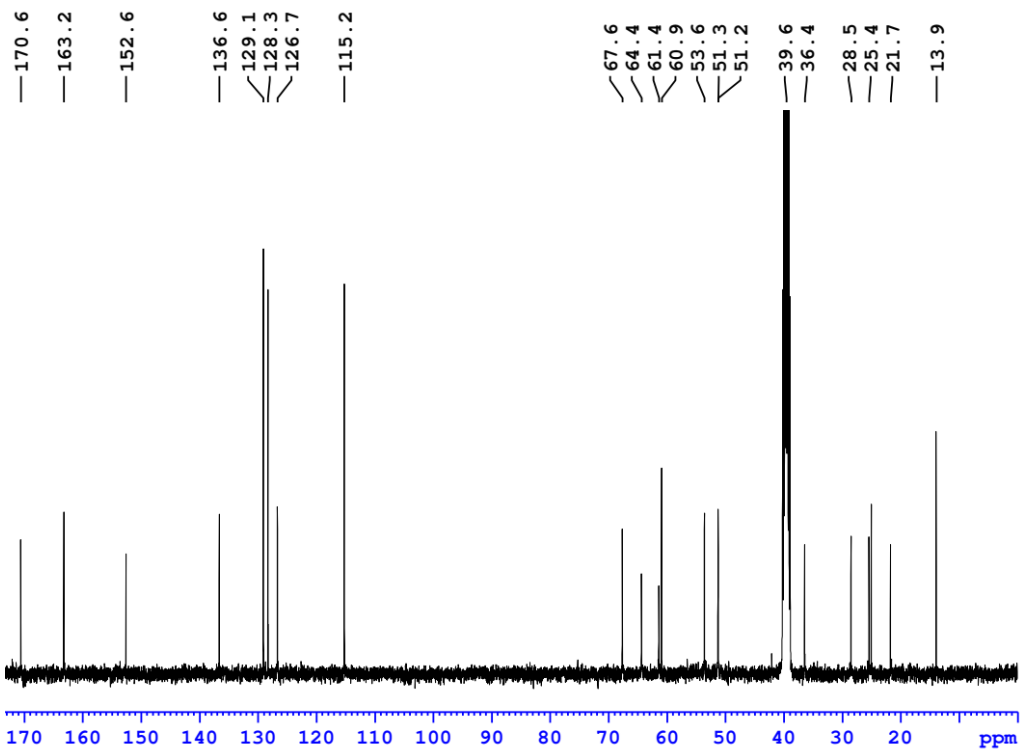

Figure S9. ^{13}C-NMR of **IAM-3**. The NMR was taken in DMSO-d_6 and the solvent peak was calibrated at the δ value of 39.52 ppm.

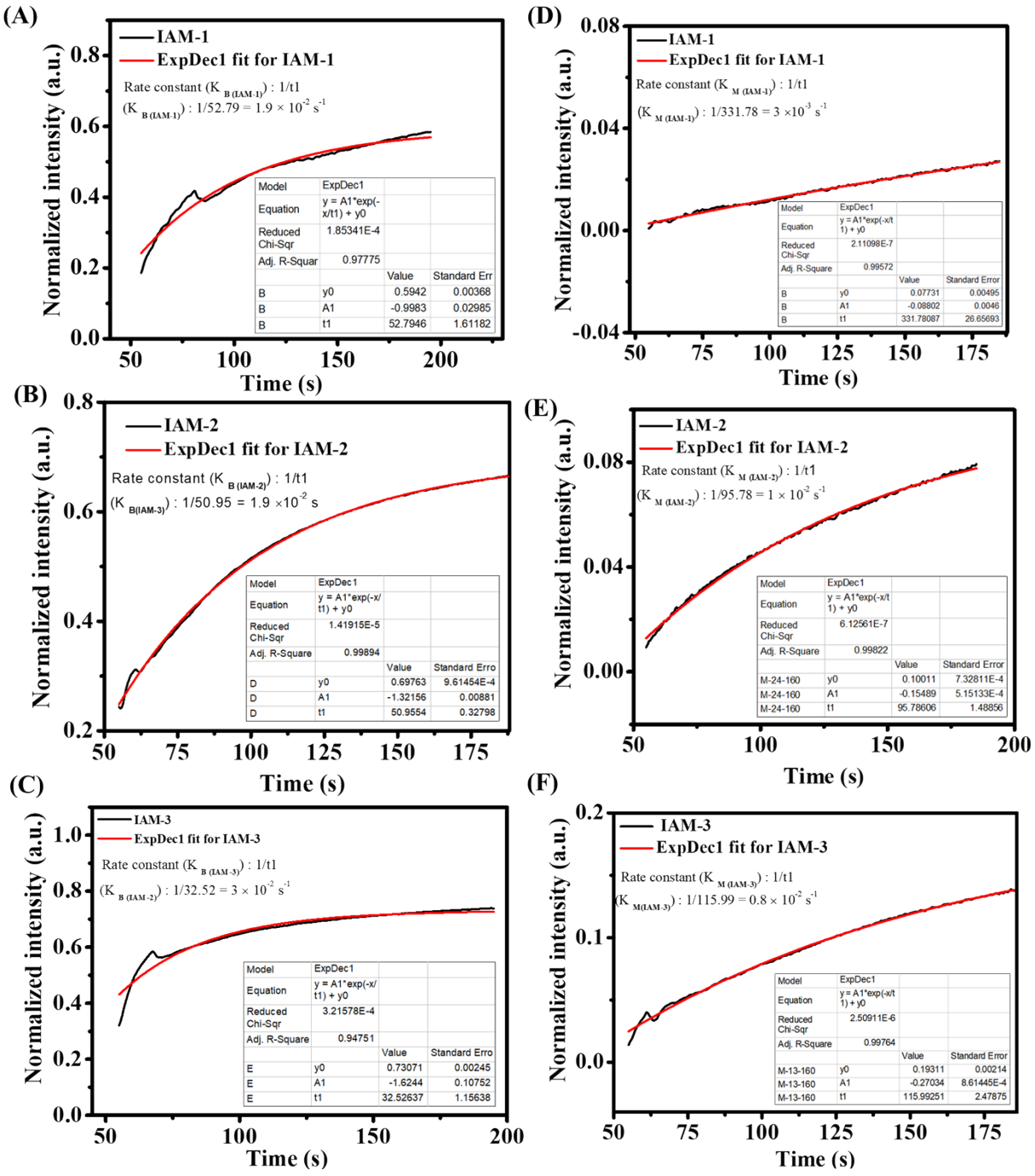

Figure S10. Representative fitting of normalized fluorescence intensity versus time plot for dye leakage assay in case of bacterial model membrane (DDPG: DPPE : 88: 12) upon treatment with (A) IAM-**1**, (B) IAM-**2** and (C) IAM-**3**. Representative fitting of normalized fluorescence intensity versus time plot for dye leakage assay in case of mammalian model membrane (DPPC) upon treatment with (A) IAM-**1**, (B) IAM-**2** and (C) IAM-**3**. Inset table shows fitting results.

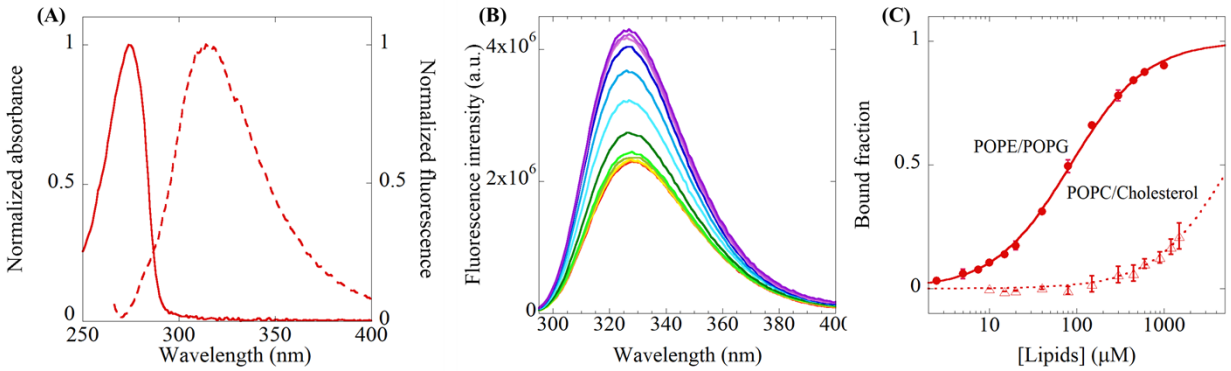

Figure S11. . (A) Normalized absorption (solid lines) and fluorescence (dashed lines) spectra of IAM-**1**. The compound concentration: 1 mM (absorbance, depending on the specific compound), 10 μM (fluorescence); water-membrane partition studies; (B) Emission spectra of IAM-**1** (10 μM) in the presence of increasing concentrations of POPE/POPG liposomes (from 0 to 1 mM, coloured from red to purple); and (C) Water-membrane partition curves with IAM-**1** [10 μM]. Filled dots and solid lines correspond to POPE/POPG 7:3 liposomes, while empty triangles and dashed lines correspond to POPC/Cholesterol 1:1 liposomes. Error bars indicate maximum error of duplicate measurements.

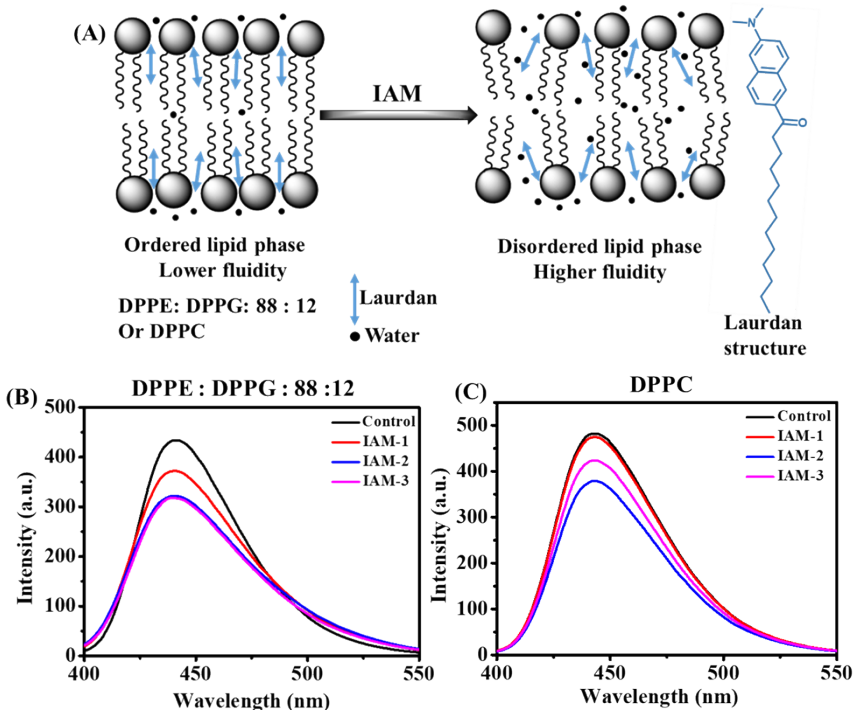

Figure S12.(A) Schematic of membrane dynamic/fluidity study using laurdan dye; (B) Change in dynamics of bacterial model membrane (DPPE: DPPG : 88: 12) upon treatment with IAMs: 1-3 at 160 µg/mL (161.1 µM) and (C) Change in dynamics of mammalian model membrane (DPPC) upon treatment with IAMs: 1-3 at 160 µg/mL (161.1 µM). Laurdan dye is well known to detect the changes in membrane fluidity. When membrane disorder allows water percolation to the region just below the head groups, where the probe is located, a spectral shift and change in intensity is observed. When the liposomes mimicking bacterial membranes were treated with IAMs **1-3** [160 µg/mL (161.1 µM)] (ortho-, meta- and para-isomers) individually, a reduction of fluorescence intensity was noticed in all the cases. This suggested that bacterial model membrane was slightly perturbed by all the positional isomers upon allowing the penetration of surrounding water molecules below the lipid head groups. Interestingly, ortho-isomer, IAM-**1** did not alter the emission spectrum of laurdan dye in case of mammalian model membrane, although it had a mild effect on bacterial model membrane. However, along with the perturbation of bacterial model membrane, IAM-**2** (meta-isomer) and IAM-**3** (para-isomer) upon interacting with mammalian model membrane decreased the fluorescence intensity.

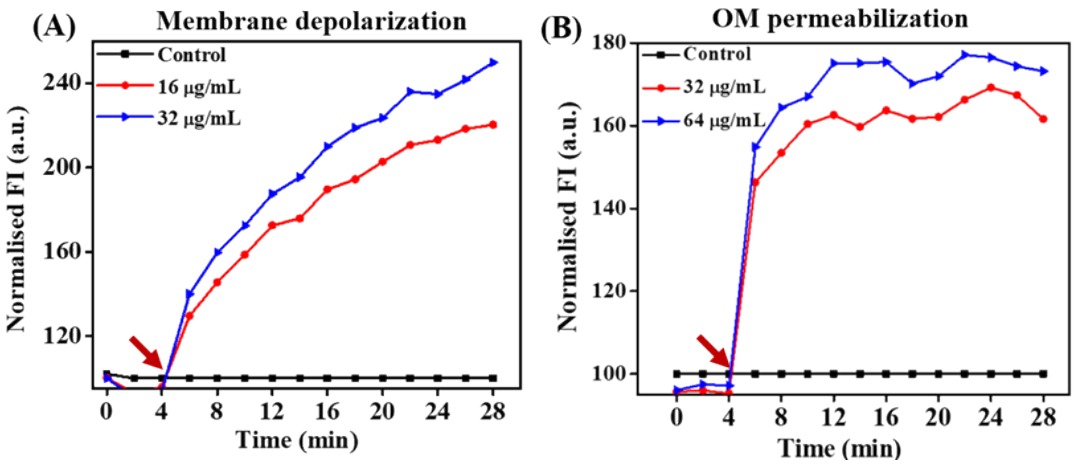

Figure S13. (A) Membrane depolarization upon IAM-**1** treatment with MRSA ATCC 33591 and (B) Outer membrane permeabilization upon IAM-**1** treatment with *E. coli* MTCC 443. The red arrow indicated the addition of IAM-**1** to the bacterial suspension.

Table 1. Antibacterial activity and hemolytic activity of isoamphipathic antibacterial molecules (IAMs: **1-3**).

Compounds	Minimum inhibitory concentration [μg/mL or (μM)]								HC_{50} (μM)
	Gram-positive bacteria						Gram-negative bacteria		
	S. aureus	MRSA	VRSA	*S. epidermidis*	*E. faecium*	VRE	*E.coli*	*A. baumannii*	
IAM-1	4 (4)	4 (4)	8 (8)	1 (1)	8 (8)	32 (32.2)	16 (16.1)	64 (64.4)	650 (654.6)
IAM-2	1 (1)	2 (2)	2 (2)	1 (1)	2 (2)	8 (8)	4 (4)	16 (16.1)	98 (98.7)
IAM-3	1 (1)	4 (4)	2 (2)	1 (1)	4 (4)	8 (8)	4 (4)	16 (16.1)	160 (161.1)
Vancomycin	1 (1)	1 (1)	1 (1)	1 (1)	1 (1)	256 (257.8)	N.D.	N.D	N.D.
Colistin	N.D.	N.D.	N.D.	N.D.	N.D.	N.D.	1 (1)	1 (1)	N.D.

Minimum inhibitory concentrations mentioned within the parenthesis are in micromolar (μM) unit.

References

1. C. Ghosh, G. B. Manjunath, P. Akkapeddi, V. Yarlagadda, J. Hoque, D. S. S. Uppu, M. M. Konai, J. Haldar, *J. Med. Chem.*, 2014, **57**, 1428–1436.
2. S. Barman, G. Dhanda, P. Naik, R. Mukherjee, L. Jolly, J. Joseph, J. Haldar, *Adv. Ther.*, 2022, doi.org/10.1002/adtp.202100234.
3. S. Barman, M. M. Konai, S. Samaddar, J. Haldar, *ACS. Appl. Mater. Interfaces*, 2019, **11**, 33559–33572.
4. F. Savini, V. Luca, A. Bocedi, R. Massoud, Y. Park, M. L. Mangoni, L. Stella, *ACS Chem. Biol.*, 2016, **12**, 52–56.

5. M. M. Konai, S. Samaddar, G. Bocchinfuso, V. Santucci, L. Stella, J. Haldar, *Chem. Commun.* 2018, **54**, 4943–4946.
6. D. S. S. M. Uppu, M. M. Konai, U. Baul, P. Singh, T. K. Siersma, S. Samaddar, S. Vemparala, L. W. Hamoen, C. Narayana, J. Haldar, *Chem. Sci.*, 2016, **7**, 4613–4623.
7. K. G. Varnava, A. S. Mohid, P. Calligari, L. Stella, J. Reynisson, A. Bhunia, V. Sarojini, *Bioconjug. Chem.*, 2019, **30**, 1998-2010.
8. J. C. M. Stewart, *Anal. Biochem.*, 1980, **104**, 10-14.
9. L. Stella, C. Mazzuca, M. Venanzi, A. Palleschi, M. Didonè, F. Formaggio, C. Toniolo, Pispisa *BiophyS. J.*,2004, **86**, 936-945.
10. A. K. Malde, L. Zuo, M. Breeze, M. Stroet, D. Poger, P. C. Nair, C. Oostenbrink, A. E. Mark, A. E. *J Chem Theory Comput.*, 2011, ***7***, 4026-4037.
11. S. Nathan, P. Andreas, C. Alexandra *et al. Eur. Biophys. J.*, 2011, **40**, 843-856.
12. E. Lindahl, M. J. Abraham, B. Hess, D. van der Spoel, *GROMACS 2020 Manual.* https://doi.org/10.5281/zenodo.3562512
13. A. Farrotti, G. Bocchinfuso, A. Palleschi, N. Rosato, E. S. Salnikov, N. Voievoda, B. Bechinger, L. Stella, *Biochim. Biophys. Acta.*, 2015, **1848**, 581-592.
14. B. Orioni, G. Bocchinfuso, J. Y. Kim, A. Palleschi, G. Grande, S. Bobone, K. S. Hahm, L. Stella, *Bioch. Biophys. Acta*, 2009, **1788**, 1523-1533.
15. G. Bocchinfuso, A. Palleschi, B. Orioni, G. Grande, F. Formaggio, C. Toniolo, L. Stella, *J. Pept. Sci.,*2009, **15**, 550-558.
16. O. Berger, O. Edholm, F. Jähnig, *Biophys. j*, 1997, **72**, 2002-2013.
17. G. Bussi, D. Donadio, M. Parrinello, Chem. Phys., 2007, **126**, 014101.
18. M. Parrinello, A. Rahman, *J. Appl. Phys.*, 1981, **52**, 7182-7190.
19. B. Hess, H. Bekker, H. J. Berendsen, J. G. Fraaije, *J. Comput. Chem.*, 1997, **18**, 1463-1472.
20. U. Essmann, L. Perera, M. L. Berkowitz, T. Darden, H. Lee, L. G. Pedersen, *Chem. Phys.*, 1995, **103**, 8577-8593.
21. E. F. Pettersen, T. D. Goddard, C. C. Huang, G. S. Couch, D. M. Greenblatt, E. C. Meng, T. E. Ferrin, *J. Comput. Chem.*, 2004, **25**, 1605-1612.